Draft version January 24, 2018
Typeset using LaTeX **twocolumn** style in AASTeX61

72 CANDIDATES AND 45 VALIDATED PLANETS FROM *K2* CAMPAIGN 10

John H. Livingston,[1,2,3] Michael Endl,[4] Fei Dai,[5,6] William D. Cochran,[4] Oscar Barragan,[7] Davide Gandolfi,[7] Teruyuki Hirano,[8] Sascha Grziwa,[9] Alexis M. S. Smith,[10] Simon Albrecht,[11] Juan Cabrera,[10] Szilard Csizmadia,[10] Jerome P. de Leon,[1] Hans Deeg,[12,13] Philipp Eigmüller,[10] Anders Erikson,[10] Mark Everett,[14] Malcolm Fridlund,[15,16] Akihiko Fukui,[17] Eike W. Guenther,[18] Artie P. Hatzes,[18] Steve Howell,[19] Judith Korth,[9] Norio Narita,[1,20,21] David Nespral,[12,13] Grzegorz Nowak,[12,13] Enric Palle,[12,13] Martin Pätzold,[9] Carina M. Persson,[16] Jorge Prieto-Arranz,[12,13] Heike Rauer,[10,22] Motohide Tamura,[1,20,21] Vincent Van Eylen,[15] and Joshua N. Winn[6]

[1] *Department of Astronomy, University of Tokyo, 7-3-1 Hongo, Bunkyo-ku, Tokyo 113-0033, Japan*
[2] *JSPS Fellow*
[3] livingston@astron.s.u-tokyo.edu
[4] *Department of Astronomy and McDonald Observatory, University of Texas at Austin, 2515 Speedway, Stop C1400, Austin, TX 78712, USA*
[5] *Department of Physics and Kavli Institute for Astrophysics and Space Research, Massachusetts Institute of Technology, Cambridge, MA, 02139, USA*
[6] *Department of Astrophysical Sciences, Princeton University, 4 Ivy Lane, Princeton, NJ 08544, USA*
[7] *Dipartimento di Fisica, Università di Torino, via P. Giuria 1, 10125 Torino, Italy*
[8] *Department of Earth and Planetary Sciences, Tokyo Institute of Technology, 2-12-1 Ookayama, Meguro-ku, Tokyo 152-8551, Japan*
[9] *Rheinisches Institut für Umweltforschung an der Universität zu Köln, Aachener Strasse 209, 50931 Köln, Germany*
[10] *Institute of Planetary Research, German Aerospace Center, Rutherfordstrasse 2, 12489 Berlin, Germany*
[11] *Stellar Astrophysics Centre, Department of Physics and Astronomy, Aarhus University, Ny Munkegade 120, DK-8000 Aarhus C, Denmark*
[12] *Instituto de Astrofísica de Canarias, C/ Vía Láctea s/n, 38205 La Laguna, Spain*
[13] *Departamento de Astrofísica, Universidad de La Laguna, 38206 La Laguna, Spain*
[14] *National Optical Astronomy Observatory, 950 North Cherry Avenue, Tucson, AZ 85719, USA*
[15] *Leiden Observatory, Leiden University, 2333CA Leiden, The Netherlands*
[16] *Department of Space, Earth and Environment, Chalmers University of Technology, Onsala Space Observatory, 439 92 Onsala, Sweden*
[17] *Okayama Astrophysical Observatory, National Astronomical Observatory of Japan, Asakuchi, Okayama 719-0232, Japan*
[18] *Thüringer Landessternwarte Tautenburg, Sternwarte 5, D-07778 Tautenberg, Germany*
[19] *Space Science and Astrobiology Division, NASA Ames Research Center, Moffett Field, CA 94035, USA*
[20] *Astrobiology Center, NINS, 2-21-1 Osawa, Mitaka, Tokyo 181-8588, Japan*
[21] *National Astronomical Observatory of Japan, NINS, 2-21-1 Osawa, Mitaka, Tokyo 181-8588, Japan*
[22] *Center for Astronomy and Astrophysics, TU Berlin, Hardenbergstr. 36, 10623 Berlin, Germany*

ABSTRACT

We present 72 planet candidates discovered in the data from the NASA *K2* mission's 10^{th} observing campaign, as well as high resolution spectroscopy and speckle imaging observations to characterize the host stars and search for stellar companions. Our analyses of these data resulted in 45 statistically validated planets, 41 of which have not been previously reported. Our validated planet sample has median values of $R_P = 2.2\ R_\oplus$, $P = 6.6$ days, $T_{\rm eq} = 850$ K, and $J = 11.2$ mag. Of particular interest are four ultra-short period planets ($P_{\rm orb} \lesssim 1$ day), 19 planets smaller than 2 $R_\oplus$, and three potential targets for atmospheric study. This sample of validated planets has enhanced the number of currently known sub-Neptunes ($R_P \approx 2$–$4R_\oplus$) and sub-Saturns ($R_P \approx 4$–$8R_\oplus$) orbiting bright stars ($J = 8$–10 mag) by ∼21% and ∼17%, respectively.

1. INTRODUCTION

The *K2* mission (Howell et al. 2014) is extending the *Kepler* legacy to a survey of the ecliptic plane, enabling the detection of transiting planets orbiting a wider range of host stars. The increased sky coverage of *K2* has enabled the detection of planets orbiting brighter host stars, as well as a larger selection of M dwarfs (Crossfield et al. 2016; Dressing et al. 2017a; Hirano et al. 2017). As a result, *K2* is yielding a large number of promising targets for follow-up studies (e.g. Vanderburg et al. 2015; Crossfield et al. 2015; Montet et al. 2015; Vanderburg et al. 2016a; Petigura et al. 2015; Vanderburg et al. 2016a,b,c; Crossfield et al. 2017). *K2* has also discovered planets in stellar cluster environments (Obermeier et al. 2016; Pepper et al. 2017; David et al. 2016b; Mann et al. 2016a, 2017a; Gaidos et al. 2017; Ciardi et al. 2017; Mann et al. 2017b; Livingston et al. 2017), including one still undergoing the process of formation (David et al. 2016a; Mann et al. 2016b).

We present here the results of our analysis of the *K2* photometric data collected during campaign 10, along with a coordinated campaign of follow-up observations to better characterize the host stars and rule out false positive scenarios. Because of campaign 10's relatively high galactic latitude, blending within the photometric apertures is less significant than for other fields, and contamination from background eclipsing binaries is low. We detect 72 planet candidates and validate 45 of them as *bona fide* planets using our observational constraints, 41 of which have not previously been reported in the literature. Our sample contains a remainder of 26 planet candidates, many of which are likely real planets.

The transit detections and follow-up observations that led to these discoveries were the result of a international collaboration called KESPRINT. Formed from the merger of two previously separate collaborations (KEST and ESPRINT), KESPRINT is focused on detecting and characterizing interesting new planet candidates from the *K2* mission (e.g. Fridlund et al. 2017; Guenther et al. 2017; Gandolfi et al. 2017; Smith et al. 2018; Niraula et al. 2017).

The rest of the paper is structured as follows. In Section 2 we describe our *K2* photometry and transit search. In Section 3 and Section 4 we describe our follow-up speckle imaging and high resolution spectroscopy of the candidates from our detection and vetting procedures. In Section 5 we describe our statistical validation framework and results. In Section 6 we discuss particular systems of interest, and we conclude with a summary in Section 7.

2. *K2* PHOTOMETRY AND TRANSIT SEARCH

Here we describe how we produce a list of vetted planet candidates from the pixel data telemetered from the *Kepler* spacecraft, as well as detailed transit modeling.

2.1. *Photometry*

In campaign 10, *K2* observed a ∼110 square degree field near the North Galactic cap from July 06, 2016 to September 20, 2016. Long cadence (30 minute) exposures of 41,607 target stars were downlinked from the spacecraft, and the data were calibrated and subsequently made available on the Mikulski Archive for Space Telescopes[1] (MAST). During the beginning of the campaign, a 3.5 pixel pointing error was detected and subsequently corrected six days after the start of observations. The data during this time is of substantially lower quality than the rest of the campaign, so we discard it in our analysis. An additional data gap was the result of the failure of detector module 4, which caused the photometer to power off for 14 days.

2.2. *Systematics*

Following the loss of two of its four reaction wheels, the *Kepler* spacecraft has been operating as *K2* (Howell et al. 2014). The dominant systematic signal in *K2* light curves is caused by the rolling motion of the spacecraft along its bore sight coupled with inter- and intra-pixel sensitivity variations. We used a method similar to that described by Vanderburg & Johnson (2014) to reduced this systematic flux variation. Our light curve production pipeline is as follows. We first downloaded the target pixel files from MAST. We laid circular apertures around the brightest pixel within the "postage stamp" (the set of pixels of the *Kepler* photometer corresponding to a given source). To obtain the centroid position of the image, we fitted 2-D Gaussian function to the aperture-summed flux distribution. We then fitted a piecewise linear function between the flux variation and the centroid motion of target. The fitted piecewise linear function was then detrended from the observed flux variation.

2.3. *Transit search*

Before searching the light curve for transits, we first removed any long-term systematic or instrumental flux variations by fitting a cubic spline to the reduced light curve from the previous section. To look for periodic transit signals, we employed the Box-Least-Squares algorithm (BLS, Kovács et al. 2002). We improved the

[1] https://archive.stsci.edu/k2/

efficiency of the original BLS algorithm by using a non-linear frequency grid that takes into account the scaling of transit duration with orbital period (Ofir 2014). We also adopted the signal detection efficiency (SDE, Ofir 2014) which quantifies the significance of a detection. SDE is defined by the amplitude of peak in the BLS spectrum normalized by the local standard deviation. We empirically set a threshold of SDE > 6.5 for the balance between completeness and false alarm rate. In order to identify all the transiting planets in the same system, we progressively re-ran BLS after removing the transit signal detected in the previous iteration.

To search for additional transit signals which may have been missed by the transit search method described above, we used two separate pipelines: one based on the DST code (Cabrera et al. 2012), and one based on the wavelet-based filter routines `VARLET` and `PHALET` (Grziwa & Pätzold 2016). This helps to ensure higher detection rates, and the number of false positives is potentially reduced by utilizing multiple diagnostics. The DST code is optimized for space-based photometry and has been successfully applied to data from CoRoT and Kepler; we ran it on the light curves extracted by Vanderburg & Johnson (2014), which are publicly available from MAST. In the wavelet-based search we first used `VARLET` to remove long-term stellar variability in the light curves, and then searched for transits using a modified version of the BLS algorithm. Detected transit-like signals were then removed using `PHALET`, which combines phase-folding and a wavelet basis to approximate periodic features. In similar fashion to the above approach, we iterate this process of feature detection and removal to enable the detection of multi-planet systems.

2.4. *Candidate vetting*

We performed a quick initial vetting to identify obvious false positives among the transiting signals identified in the previous section. Planetary candidates that survived the various tests were followed up with speckle imaging and reconnaissance spectra for proper statistical validation. We tested for the presence of any "odd-even" variations and significant secondary eclipse, both of which are likely signatures of eclipsing binaries. The odd-even effect is the variation of the eclipse depth between the primary and secondary eclipse of an eclipsing binary. If mistaken for planetary transits, the primary and secondary eclipses will be the odd and even numbered transits.

We fitted Mandel & Agol (2002) model to the odd and even transits separately. If a systems shows odd-even variations with more than 3-σ significance, it is flagged as a false positive. We also looked for any secondary eclipse in the light curve. We use the Mandel & Agol (2002) model fit of the transits as a template for the occultation. The time of opposition was allowed to vary freely. We set the limb darkening coefficient to be 0. We fixed all other transit parameters. If a system shows a secondary eclipse with more than 3-σ significance, we calculated the geometric albedo using the depth of secondary eclipse. The object is likely self-luminous, hence likely a false positive, if the albedo is much greater than 1.

2.5. *Stellar rotation periods*

We also measured stellar rotation periods $P_{\rm rot}$ from the variability in the light curves induced by starspot modulation. About half of the light curves of our candidates exhibited a lack of rotational modulation, or the $\sim$ 80 day *K2* time-series was not long enough to constrain the period. For the rest, we used the autocorrelation function (ACF; e.g. McQuillan et al. 2014) to measure the rotational period, and we include these results in Table 1 along with initial estimates of the basic transit parameters of each candidate. To help ensure the validity of these measurements, we also used the Lomb-Scargle periodogram (Lomb 1976; Scargle 1982) to measure the rotational periods, and the results were in good agreement.

Table 1. Candidate planets detected in *K2* Campaign 10.

EPIC	K_p [mag]	P [days]	T_0 [BKJD]	T_{14} [hours]	Depth	$P_{\rm rot}$ [days]
201092629	11.858	26.80960	2751.22301	4.1	0.00090	22^{+6}_{-2}
201102594	15.615	6.51362	2753.24355	2.0	0.00624	25±3
201110617	12.947	0.81312	2750.14280	1.3	0.00029	16.8±2.5
201111557	11.363	2.30190	2750.16887	1.9	0.02268	12.0±1.8
201127519	11.558	6.17888	2752.54744	2.5	0.01303	—
201128338	13.114	32.65514	2775.61538	4.0	0.00159	15.6±2.2
201132684	11.678	10.06144	2757.49129	3.8	0.00070	13.8±1.3
201132684	11.678	5.90644	2750.82393	5.0	0.00015	13.8±1.3
201164625	11.919	2.71130	2750.15415	3.1	0.00020	12.5±1.5
201166680	10.897	24.94102	2751.50642	5.2	0.00019	—
201166680	10.897	11.54026	2760.21567	3.7	0.00016	—
201180665	13.080	17.77293	2753.49860	2.9	0.03662	—
201211526	11.696	21.06972	2755.47681	3.9	0.00030	—
201225286	11.729	12.42045	2753.51656	3.3	0.00065	20.8±1.6
201274010	13.902	13.00848	2756.51285	2.2	0.00065	—
201352100	12.798	13.38331	2761.79018	2.2	0.00120	36±11
201357643	11.998	11.89285	2754.55139	4.2	0.00107	—
201386739	14.423	5.76673	2750.69809	3.4	0.00134	35±6
201390048	11.961	9.45476	2750.91805	3.0	0.02669	—
201390927	14.210	2.63769	2750.34486	1.7	0.00110	—
201392505	13.384	27.46268	2759.08065	5.5	0.00150	—
201437844	9.234	21.05691	2757.07463	4.4	0.00100	—
201437844	9.234	9.56041	2753.52336	3.5	0.00030	—
201595106	11.678	0.87716	2750.04678	1.0	0.00025	—
201598502	14.331	7.51477	2755.43276	2.3	0.00129	—
201615463	11.964	8.52695	2753.77012	3.7	0.00016	—

Table 1 continued

Table 1 *(continued)*

EPIC	K_p [mag]	P [days]	T_0 [BKJD]	T_{14} [hours]	Depth	$P_{\rm rot}$ [days]
228707509	14.806	15.35097	2752.50970	3.6	0.02386	—
228720681	13.763	15.78172	2753.41768	3.4	0.01028	9.8±1.1
228721452	11.325	4.56306	2749.97654	2.8	0.00020	—
228721452	11.325	0.50564	2750.56402	0.9	0.00010	—
228724899	13.293	5.20262	2753.45425	1.4	0.00113	—
228725791	14.344	6.49166	2755.15309	1.7	0.00110	32±3
228725791	14.344	2.25063	2749.97225	1.2	0.00100	32±3
228725972	12.482	4.47742	2752.68823	2.4	0.03270	—
228725972	12.482	10.09607	2755.40514	3.6	0.05928	—
228729473	11.524	16.77295	2752.76308	12.4	0.00199	36^{+5}_{-3}
228732031	11.937	0.36933	2749.93377	1.0	0.00040	9.4±1.9
228734900	11.535	15.87196	2754.36634	4.6	0.00034	—
228735255	12.483	6.56919	2755.28506	3.3	0.01280	31.1±2.0
228736155	12.042	3.27138	2751.02175	2.4	0.00027	—
228739306	13.318	7.17183	2755.10828	2.8	0.00070	—
228748383	12.459	12.40924	2750.04443	5.9	0.00024	—
228748826	13.948	4.01391	2751.12580	2.4	0.00102	39^{+6}_{-8}
228753871	13.190	18.69262	2757.73955	2.2	0.00082	16.4±2.3
228758778	14.806	9.30064	2756.07251	2.7	0.00214	—
228758948	12.866	12.20296	2753.82771	4.0	0.00128	11.3±1.7
228763938	12.640	13.81369	2763.19176	3.6	0.00036	—
228784812	12.613	4.18851	2751.01722	2.2	0.00014	—
228798746	12.660	2.69742	2750.20390	1.5	0.02587	—
228801451	10.955	8.32531	2753.35291	2.5	0.05325	19.5±2.7
228801451	10.955	0.58429	2750.46482	1.5	0.01625	19.5±2.7
228804845	12.551	2.85966	2749.60073	2.6	0.00020	—
228809391	12.595	19.57977	2763.80171	2.6	0.00100	—
228809550	14.665	4.00152	2751.00014	2.1	0.01259	—
228834632	14.887	11.72953	2758.63317	2.1	0.00111	23.6±2.1
228836835	14.925	0.72813	2750.25925	0.8	0.00068	—
228846243	14.505	25.55355	2756.93232	5.4	0.00220	—
228849382	13.765	12.11974	2757.60783	2.4	0.00120	—
228849382	13.765	4.09724	2749.96191	1.6	0.00052	—
228888935	14.103	5.69090	2751.66837	3.3	0.00533	7.2±1.1
228894622	13.319	1.96389	2750.30878	1.1	0.00183	20.8±2.4
228934525	13.351	7.95451	2751.33782	2.1	0.00110	28.3±3.1
228934525	13.351	3.67622	2752.05420	1.7	0.00110	28.3±3.1
228964773	14.948	37.20866	2776.75812	3.1	0.00280	—
228968232	14.659	5.51999	2753.52223	3.6	0.00097	—
228974324	12.873	1.60586	2750.28938	1.3	0.00034	22.0±2.3
228974907	9.344	20.78234	2759.63865	5.0	0.00010	—
229004835	10.151	16.13753	2764.62816	2.1	0.00036	22.2±2.5
229017395	13.163	19.09913	2753.28329	6.0	0.00049	—
229103251	13.680	11.66653	2756.71784	3.1	0.00114	—
229131722	12.515	15.47996	2752.70980	4.2	0.00037	—
229133720	11.477	4.03683	2750.96360	1.5	0.00091	11.8±1.3

2.6. *Transit modeling*

We used the orbital period, mid-transit time, transit depth, and transit duration identified by BLS as the starting points for more detailed transit modeling. The transit light curve was generated by the `Python` package `Batman` (Kreidberg 2015). To reduce the data volume, we only use the light curve in a $3\times T_{14}$ window centered on the mid-transit times. We first tested if any of the systems showed strong transit timing variations (TTVs). We used the Python interface to the Levenberg-Marquardt non-linear least squares algorithm `lmfit` (Newville et al. 2014) to find the best-fit model of the phase-folded transit, and then fit this template to each transit separately to identify individual transit times of each candidate. Since none of the system presented in this work showed significant TTVs within the ∼80 days of *K2* observation, we assumed linear ephemerides in subsequent analyses.

The transit parameters in our linear ephemeris model include the orbital period $P_{\rm orb}$, the mid-transit time T_0, the planet-to-star radius ratio $R_P/R_\star$, the scaled orbital distance $a/R_\star$, the impact parameter $b \equiv a\cos i/R_\star$, and the transformed quadratic limb-darkening coefficients q_1 and q_2. We imposed Gaussian priors on the limb-darkening coefficients (i.e. in the non-transformed parameter space, u_1 and u_2). To determine the location and width of these priors, we used a Monte Carlo method to sample the stellar parameters of each candidate host star ($T_{\rm eff}$, $\log g$, and [Fe/H]), and then used these to derive distributions of u_1 and u_2 from an interpolated grid based on the limb-darkening cofficients for the Kepler bandpass tabulated by Claret et al. (2012)[2]. We used the median and standard deviation of these distributions to define the Gaussian limb-darkening priors, and used uniform priors for all other parameters. To account for the 30 min integration time of long cadence *K2* photometry, we used the built-in feature of `Batman` to super-sample the model light curve by a factor of 16 before averaging every 30 min window (Kipping 2010).

We adopted a Gaussian likelihood function, and found the maximum likelihood solution using `scipy.optimize` (Jones et al. 2001–present). We then sampled the joint posterior distribution using `emcee` (Foreman-Mackey et al. 2013), a Python implementation of the affine-invariant Markov Chain Monte Carlo ensemble sampler (Goodman & Weare 2010). We launched 100 walkers in the vicinity of the maximum likelihood solution and ran the sampler for 5000 steps, discarding the first 1000 as "burn-in." To ensure that the resultant marginalized posterior distributions consisted of 1000's of independent samples (enough for negligible sampling error) we computed the autocorrelation length scale of each parameter, and visual inspection revealed the posteriors to be smooth and unimodal. We summarize the transit parameter posterior distributions in Table 6 using the 16^{th}, 50^{th}, and 84^{th} percentiles, and we use the posterior samples to compute other quantities of interest throughout this work (i.e. R_P, $T_{\rm eq}$). The phase-folded light curves of the candidates are shown in Figure 1 and Figure 2, with best-fitting transit model and 68% credible region over-plotted.

[2] https://github.com/john-livingston/limbdark

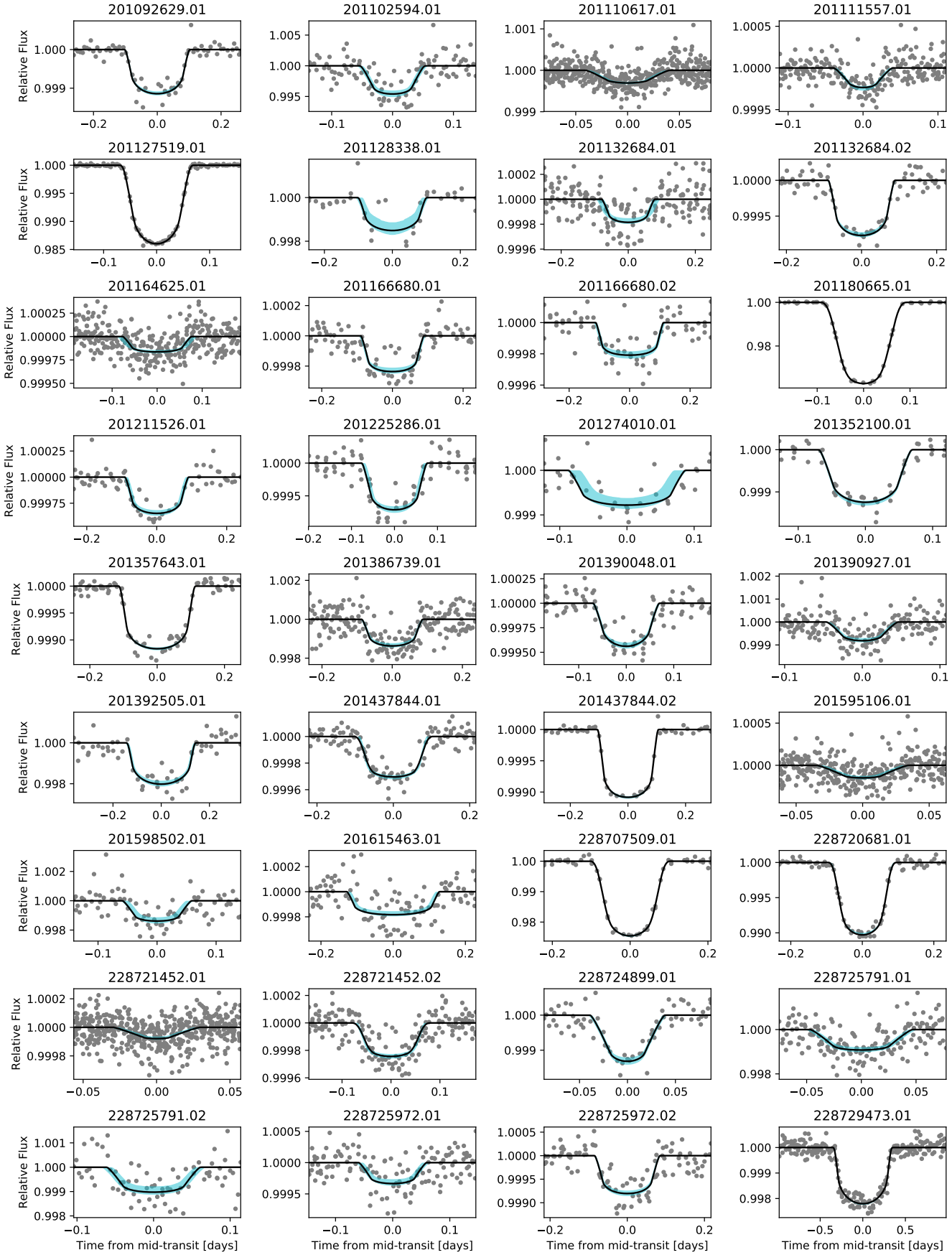

Figure 1. Phase-folded transits (gray), with the maximum *a posteriori* transit model (black) and 68% credible region (light blue) overplotted.

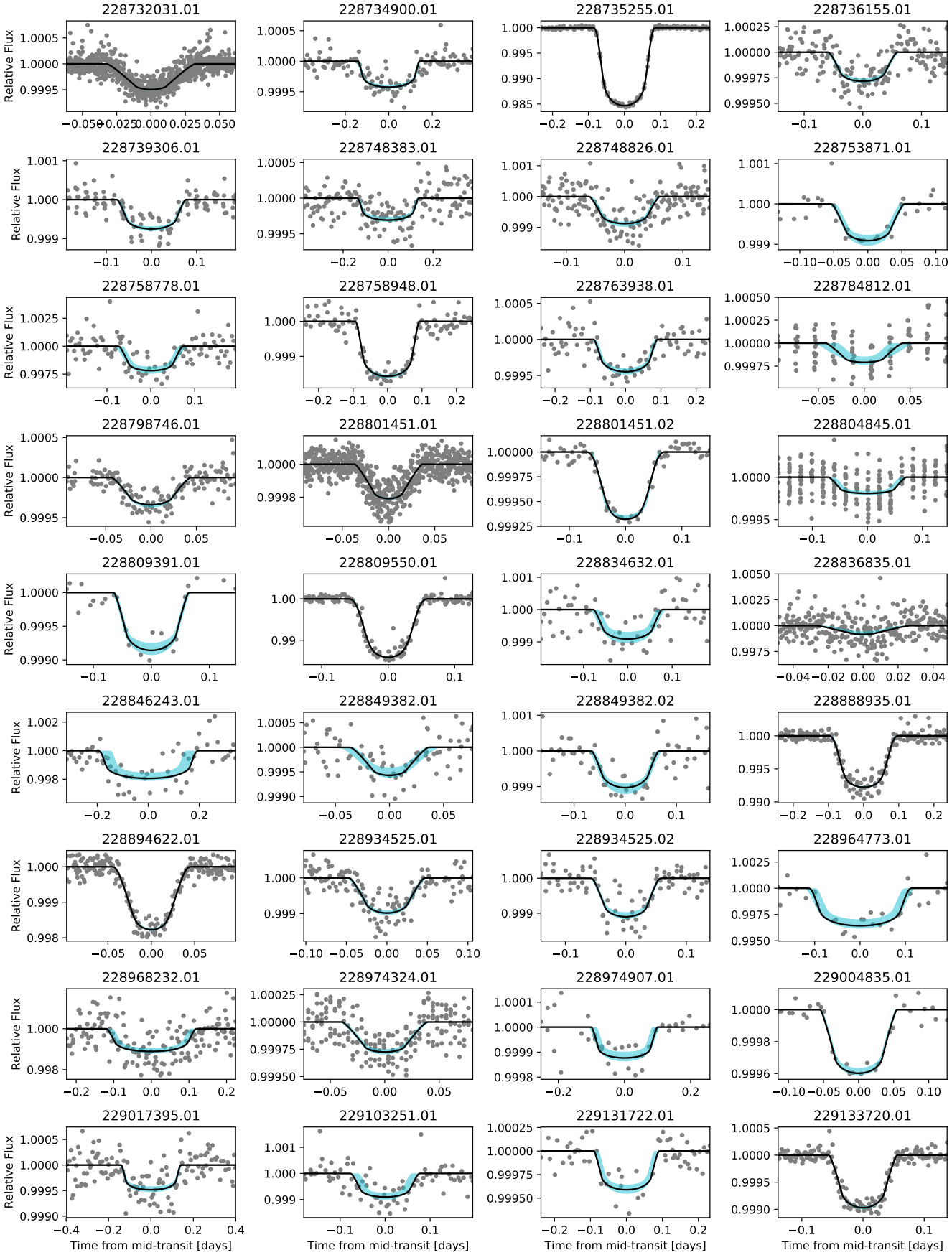

Figure 2. Continuation of Figure 1.

3. SPECKLE IMAGING

We observed candidate host stars with the NASA Exoplanet Star and Speckle Imager (NESSI) on the 3.5-m WIYN telescope at the Kitt Peak National Observatory. NESSI is a new instrument that uses high-speed electron-multiplying CCDs (EMCCDs) to capture sequences of 40 ms exposures simultaneously in two bands (Scott et al. (2016), Scott et al., in prep.). Data were collected following the procedures described by Howell et al. (2011). We conducted all observations in two bands simultaneously: a 'blue' band centered at 562nm with a width of 44nm, and a 'red' band centered at 832nm with a width of 40nm. The pixel scales of the 'blue' and 'red' EMCCDs are 0.0175649″ and 0.0181887″ per pixel, respectively. We make all of our speckle imaging data publicly available via the community portal ExoFOP[3]. We list the individual NESSI data products used in this work in Table 9.

Speckle imaging data were reduced following the procedures described by Howell et al. (2011), resulting in diffraction limited 4.6″ × 4.6″ reconstructed images (256 × 256 pixels) of each target star. The methodology has been described in detail in previous works (e.g. Horch et al. 2009, 2012, 2017), but we provide a brief review here for convenience.

First, the autocorrelation function of each 40 ms exposure is summed and Fourier transformed, resulting in the average spatial frequency power spectrum. The speckle transfer function is then deconvolved by dividing the target's power spectrum by that of the corresponding point source calibrator, yielding the square of the modulus estimate of the target's Fourier transform. The phase information can then be recovered from bispectral analysis, as first described by Lohmann et al. (1983). This is accomplished by computing the Fourier transform of the summed triple correlation function of the exposures, which in combination with the modulus estimate yields the complex Fourier transform of the target. This is then filtered with a low-pass 2-d Gaussian before being inverse transformed, yielding the reconstructed image.

We extract background sensitivity limits from the reconstructed images by computing the mean and standard deviation of a series of concentric annuli centered on the target star, as described by Howell et al. (2011). The then compute contrast curves by fitting a cubic spline to the kernel-smoothed 5-σ sensitivity limits, expressed as a magnitude difference relative to the target star as a function of radius. For stars of moderate brightness ($V = 10 - 12$ mag) we typically achieve contrasts of ~ 4 magnitudes at 0.2″. See Figure 3 for a plot showing all of the contrast curves obtained in this work. We detect 4 candidate host stars with secondaries, see Table 2.

[3] https://exofop.ipac.caltech.edu

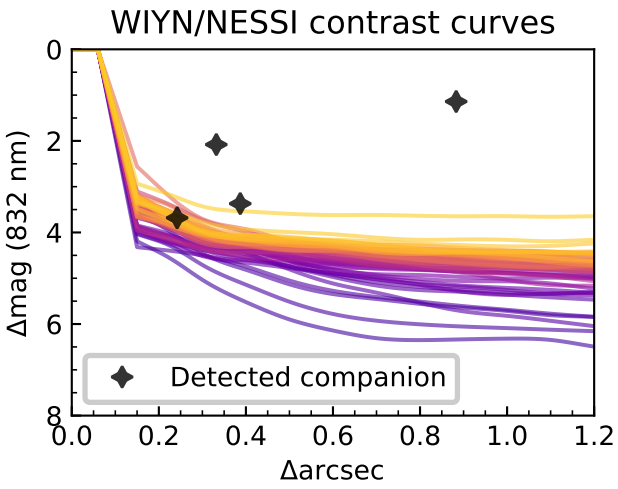

Figure 3. Contrast curves and detected companions

Table 2. Stars with detected companions. All detections made in the 832nm band. Note a: The quadrant of the position angle is ambiguous, meaning it could be off by exactly 180 degrees. Note b: The binary model fit is of poor quality, so uncertainty may be larger than typical.

EPIC	Δarcsec	Δmag	θ [deg. E of N]	Note
201352100	0.387	3.37	312.054	a
201390927	0.883	1.14	341.286	a
201392505	0.242	3.68	42.491	b
228964773	0.332	2.08	43.499	b

4. HIGH RESOLUTION SPECTROSCOPY

4.1. *McDonald/Tull*

Most of the high resolution spectra presented in this paper were obtained with the Tull Coudé cross-dispersed echelle spectrograph (Tull et al. 1995) at the Harlan J. Smith 2.7m telescope at McDonald Observatory. Observations were conducted with the 1.2×8.2″ slit, yielding a resolving power of $R \sim 60,000$. The spectra cover 375-1020 nm, with increasingly larger inter-order gaps longward of 570 nm. For each target star, we obtained three successive short exposures in order to allow removal of energetic particle hits on the CCD detector. We used an exposure meter to obtain an accurate flux-weighted barycentric correction and to give an exposure length

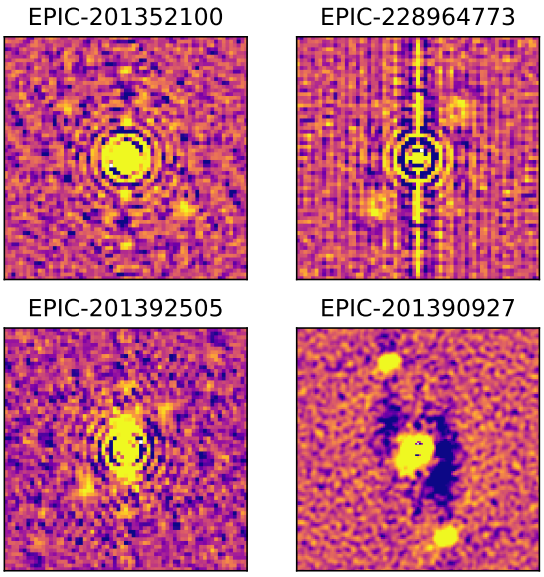

Figure 4. Reconstructed 832nm images of stars with detected companions. FOV widths shown are 1.16″, except for EPIC-201390927, which has a FOV of 2.33″.

that resulted in a signal/noise ratio of about 30 per pixel. Bracketing exposures of a Th-Ar hollow cathode lamp were obtained in order to generate a wavelength calibration and to remove spectrograph drifts. This enabled calculation of absolute radial velocities from the spectra. The raw data were processed using IRAF routines to remove the bias level, inter-order scattered light, and pixel-to-pixel ("flat field") CCD sensitivity variations. We traced the apertures for each spectral order and used an optimal extraction algorithm to obtain the detected stellar flux as a function of wavelength.

We computed stellar parameters from our reconnaissance Tull spectra using *Kea* (Endl & Cochran 2016). In brief, we used standard IRAF routines to perform flat fielding, bias subtraction, and order extraction, and we used a blaze function determined from high SNR flat field exposures to correct for curvature induced by the blaze. *Kea* uses a large grid of synthetic model stellar spectra to compute stellar effective temperatures, surface gravities, and metallicities. See Table 7 for the stellar parameters used in this work. From a comparison with higher S/N spectra obtained with Keck/HIRES we found typical uncertainties of 100 K in $T_{\rm eff}$, 0.12 dex in [Fe/H], and 0.18 dex in $\log g$. For a detailed description of Kea see Endl & Cochran (2016).

4.2. *NOT/FIES*

We also used the FIbre-fed Échelle Spectrograph (FIES; Frandsen & Lindberg 1999; Telting et al. 2014) on the 2.56-m Nordic Optical Telescope (NOT) of Roque de los Muchachos Observatory (La Palma, Spain) to collect high-resolution ($R \approx 67\,000$) spectra for four campaign 10 candidates (EPIC-228729473, EPIC-228735255 = K2-140, EPIC-201127519, and EPIC-228732031 = K2-131). The observations were carried out between February 15 to May 23, 2017 UTC, within observing programs 54-027, 55-019, and 55-202. We followed the same strategy as in Gandolfi et al. (2013) and traced the RV drift of the instrument by bracketing the science exposures with 90-sec ThAr spectra. We reduced the data using standard IRAF routines and extracted the RVs via multi-order cross-correlations using different RV standard stars observed with the same instrument.

4.3. *TNG/HARPS-N*

We observed EPIC-228801451, EPIC-228732031 (aka K2-131 Dai et al. 2017), EPIC-201595106, and EPIC-201437844 = K2-109 (aka HD 106315; Crossfield et al. 2017; Rodriguez et al. 2017) with the HARPS-N spectrograph ($R \approx 115000$; Cosentino et al. 2012) mounted at the 3.58 m Telescopio Nazionale Galileo (TNG) of Roque de los Muchachos Observatory (La Palma, Spain). The observations were performed in January 2017 as part of observing programs A34TAC_10 and A34TAC_44. We reduced the data using the dedicated off-line pipeline and extracted the RVs by cross-correlating the échelle spectra with a G2 numerical mask. The HARPS-N data of EPIC-228732031 (K2-131) have been published by our team in Dai et al. (2017). We refer the reader to that paper for a detailed description and analysis of the data. We list the results of our analysis of these spectra in Table 10.

4.4. *Stellar properties*

To estimate host star properties of interest, such as stellar radii and luminosities, we utilize isochrone models in conjunction with the stellar parameters for each host star. These stellar parameters are derived primarily from our spectroscopic observations (see previous sections), and for those stars which lack spectroscopically-derived stellar parameters, we rely on the parameters of Huber et al. (2016, hereafter H16) . In conjunction with available broadband photometry, we estimate physical stellar parameters directly from the effective temperature $T_{\rm eff}$, surface gravity $\log g$, and metallicity [Fe/H] of each star. We utilize the `isochrones` (Morton 2015a) interface to the Dartmouth stellar model grid (Dotter et al. 2008) to estimate these parameters and their uncertainties using the `MultiNest` sampling algorithm (Feroz et al. 2013). We note, however, that the stellar radii of the M dwarfs in the sample from H16 may be understimated (see e.g. Dressing et al. 2017b). See Table 7 for a full list of the stellar parameters we derive or utilize in this work.

We also performed the spectral analyses for the targets (EPIC-201127519, EPIC-201437844 = K2-109, EPIC-201595106, EPIC-228801451) observed with FIES and HARPS-N using `SpecMatch-emp` developed by Yee et al. (2017). In the code, the input spectra are fitted to hundreds of library template spectra collected by the California Planet Search, and the stellar parameters ($T_{\rm eff}$, $R_\star$, and [Fe/H]) are estimated based on the interpolation of the parameters for best-matched library stars. Among them EPIC-201127519, EPIC-201595106, and EPIC-228801451 were also observed with the Tull spectrograph, and the resulting parameters by `SpecMatch-emp` are in agreement within $\sim 1.5\sigma$ with those estimated from the Tull spectra by the *Kea* code. But to characterize the candidate-hosting stars as uniformly as possible, we adopt the spectroscopic parameters by *Kea* in Table 7 and in the subsequent discussion. For K2-109, we obtained $T_{\rm eff} = 6326 \pm 110$ K, $R_\star = 1.86 \pm 0.30\ R_\odot$, and [Fe/H] $= -0.20 \pm 0.08$. While $T_{\rm eff}$ and [Fe/H] agrees within 1-σ with the literature values (Rodriguez et al. 2017; Crossfield et al. 2017), $R_\star$ exhibits a moderate disagreement with that in the literature ($R_\star = 1.281^{+0.051}_{-0.058}$ $R_\odot$ Rodriguez et al. 2017). This is probably due to the small number of library stars in `SpecMatch-emp` in the region with $T_{\rm eff} > 6300$ K, but this disagreement does not have any impact on our results.

5. PLANET VALIDATION

5.1. *Statistical framework*

We use the open source `vespa` software package (Morton 2012, 2015b) to compute the false positive probabilities (FPPs) of each planet candidate. `vespa` uses the `TRILEGAL` Galaxy model (Girardi et al. 2005) to compute the posterior probabilities of both planetary and non-planetary scenarios given the observational constraints, and considers false positive scenarios involving simple eclipsing binaries, blended background eclipsing binaries, and hierarchical triple systems. `vespa` models the physical properties of the host star, taking into account any available broadband photometry and spectroscopic stellar parameters, and compares a large number of simulated scenarios to the observed phase-folded light curve. Both the size of the photometric aperture and contrast curve constraints are accounted for in the calculations, as well as any other observational constraints such as the maximum depth of secondary eclipses allowed by the data. We adopt a fiducial validation criterion of FPP < 0.01, which is reasonably conservative and also consistent with the literature (e.g. Montet et al. 2015; Crossfield et al. 2016; Morton et al. 2016). We tabulate candidate parameters along with their FPPs in Table 6, and the full `vespa` likelihoods are listed in Table 8.

All of the candidates we detect in multi-planet systems meet the fiducial validation criterion of FPP $<$ 1%. However, FPPs computed with `vespa` treat only the individual planet candidates in isolation, and thus do not take into account any multiplicity in each system. Stars with multiple transiting planet candidates have been shown to exhibit a near-zero false positive rate (Lissauer et al. 2011, 2012, 2014). For this reason we apply a "multiplicity boost" factor to the planet probability appropriate for each candidate in a multi-planet system. Lissauer et al. (2012) estimated a multiplicity boost factor of 25 for systems containing 2 planet candidates in the *Kepler* field, and we apply the same factor in this work. To check that this factor is appropriate for *K2* campaign 10, we follow Sinukoff et al. (2016) and utilize equations (2) and (4) of Lissauer et al. (2012) to estimate the sample purity $P = {\rm FPP}_{int}/n_{cand}$, where ${\rm FPP}_{int}$ is the integrated FPP of our sample and n_{cand} is the number of planet candidates we detect (72). This estimate of P is quite high ($\sim 95\%$), perhaps due to a lack of contamination from background stars due to the high galactic latitude of the field, or due to our team's vetting procedures. The fraction of detected planet candidates in multi-systems (18/72) in conjunction with the high sample purity yields a multiplicity boost which is significantly higher than the factor of 25 estimated by Lissauer et al. (2012) for the *Kepler* field. Although the true value is likely to be higher, we conservatively apply only a factor of 25, consistent with Lissauer et al. (2012), and the FPPs in Table 6 reflect this accordingly.

5.2. *Stellar companions*

To ensure that the FPPs computed by `vespa` are reliable, we take into account the presence of any nearby stars detected in speckle or archival imaging. Table 2 lists the nearby stars we detected via speckle imagine, along with their separations and delta-magnitudes relative to the primary stars. Figure 4 shows the reconstructed speckle images for these stars, and Figure 3 shows these detections relative to the ensemble of contrast curves from all of our speckle images. Table 3 lists those stars found in the EPIC to be near and bright enough to be the source of the observed transit signals.

5.2.1. *Companions detected in high resolution imaging*

On the nights of 2017-03-15, 2017-03-17, and 2017-03-18 we acquired speckle imaging of EPIC-201352100, EPIC-201390927, EPIC-201392505, and EPIC-228964773 (see Table 9). We detected companions in the reconstructed images (see Figure 4), so we assessed the possibility that the transit signal might not originate from

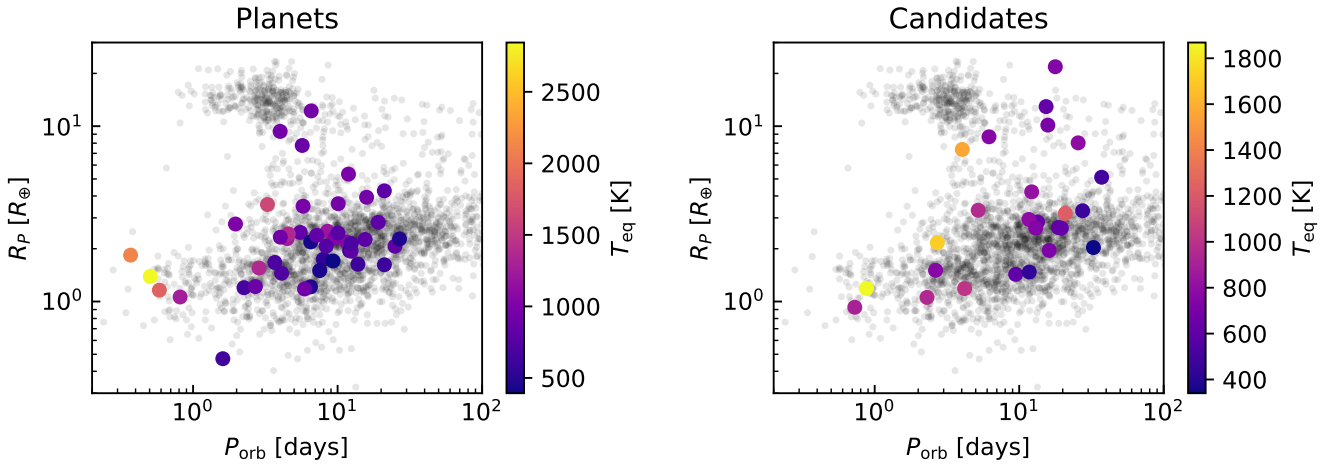

Figure 5. Validated (left) and candidate (right) planets from Campaign 10 against the background of previously confirmed planets, colored by their equilibrium temperature (assuming a Bond albedo of 0.3).

the primary stars. We used the following relation between the observed transit depth δ' and the true transit depth δ in the presence of dilution from a companion Δm magnitudes fainter than the primary star:

$$\delta' = \frac{\delta}{1 + 10^{0.4\Delta m}} \quad (1)$$

Assuming a maximum eclipse depth of 100% (i.e. a brown dwarf — M dwarf binary) we can potentially rule out the secondary star as the source of the observed signal. For shallower transits the maximum allowed dilution from the primary is larger, and therefore even a relatively faint secondary source cannot be ruled out as the host. For each of these four of these candidates, the secondary source is bright enough (given the observed transit depth) that we cannot rule out the possibility they are the source of the signal (see Table 2). For this reason, we do not validate any of these candidates as planets, as we do not know the true source of the signal (and therefore the true planet size), even though they all have low FPPs.

5.2.2. *Companions in the EPIC*

In addition to analyzing the scenarios involving companions detected in high resolution speckle imaging, we also performed a search of the EPIC for any additional stars within the photometric apertures which could be the source of the observed signals. Most of these queries yielded no stars within the aperture other than the primary, but there were some cases in which the query yielded a star bright enough to be the source of the observed transit signal; we list these cases in Table 3. Despite their low FPPs, we do not validate these candidates because we do not know which star is the true host. As we expect most of these candidates to be genuine planets, they present good validation opportunities via higher angular resolution follow-up transit observations, either from the ground or from space (i.e. with *Spitzer* or *CHEOPS*).

Table 3. EPIC sources within the photometric apertures which are bright enough to produce the observed transit-like signals.

EPIC	Contaminant	ρ [arcsec]	ΔK_p [mag]
201111557	201111694	15.90	5.187
201164625	201164669	17.58	3.228
201595106	201595004	13.62	5.839
228707509	228707572	12.48	1.563
228720681	228720649	7.86	2.905
228758948	228758983	9.00	3.267

5.3. *Pipeline comparison*

As an additional check on the quality of the candidates, we performed a parallel analysis using light curves from an independent *K2* pipeline. We first downloaded the light curves of Vanderburg & Johnson (2014) from MAST for all the targets listed in Table 1, then detrended the light curves by fitting a second order polynomial to the out-of-transit data using `exotrending` (Barragán & Gandolfi 2017). To explore the transit model parameter space with MCMC, we used `pyaneti` (Barragán et al. 2017a) to fit the detrended light curves with uniform priors for all parameters; more description of the `pyaneti` MCMC evolution and parameter estimation can be found in Barragán et al. (2017b) and

Gandolfi et al. (2017). For the majority of candidates, the main transit parameters of interest (P, $R_P/R_\star$, b, and a/rstar) are consistent within 1-σ between our two independent analyses, although there are some cases in which marginally significant differences were found. These differences are likely to be the result of different handling of the *K2* systematics and/or the stellar variability in the light curves. The overall excellent agreement between these two independently-derived sets of transit parameters provides an additional layer of confidence in the quality of the candidates. The results of this comparison are listed in Table 12.

5.4. *Validated planets*

We validate 45 planets out of our sample of 72 candidates, and tabulate the FPPs along with parameter estimates of interest in Table 6. Of the 45 validated planets we report here, four of them have been proviously reported in the literature: EPIC-201437844bc = K2-109bc (Crossfield et al. 2017; Rodriguez et al. 2017), EPIC-228732031b = K2-131b (Dai et al. 2017), and EPIC-228735255b = K2-140b Giles et al. (2017). In the left panel of Figure 5 we plot the planetary radii, orbital periods, and equilibrium temperatures of the validated planets in the sample.

We investigated the impact of these new planets to the population of currently known planets by querying the NASA Exoplanet Archive[4] (Akeson et al. 2013). We computed the fractional enhancement to the known population due to the 45 planets as a function of planet size and host star brightness (see Figure 6). As of January 22, 2018, the populations of sub-Neptunes ($R_P \approx 2$–$4R_\oplus$) and sub-Saturns ($R_P \approx 4$–$8R_\oplus$) orbiting bright stars ($J = 8$–10 mag) are ehanced by ∼21% and ∼17%, respectively. Because of the brightness of the host stars, many of these planets are ideal for detailed characterization studies via precision Doppler and transmission spectroscopy, which we discuss in greater detail in Section 6.2.

5.5. *Candidates*

Out of the 72 planet candidates we present here, 26 are not validated. Most cannot be validated due to the FPP being above our fiducial validation criterion of 1% or the presence of a contaminating star within the photometric aperture. See Table 8 for the likelihoods of various false positive scenarios and the planet scenario, as computed by `vespa`. There are several candidates which we do not validate for other reasons, which we discuss below. In the right panel of Figure 5 we plot the planetary radii, orbital periods, and equilibrium temperatures of the non-validated candidates.

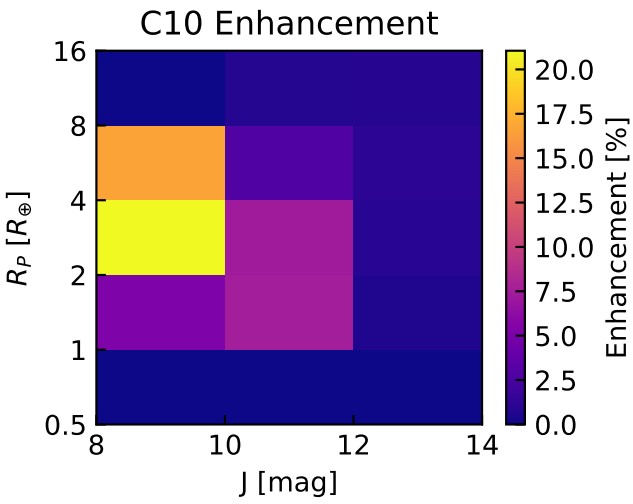

Figure 6. The fractional enhancement to the population of previously confirmed planets from our sample of 45 validated C10 planets.

The candidate 228729473.01 exhibits a long transit duration, and also has the highest FPP of any candidate in our sample (> 75%). Subsequent spectroscopic analyses revealed large RV variations which are consistent with the candidate being a false positive involving an M dwarf eclipsing a sub-giant, see Csizmadia et al (in prep.) for more details. The light curve of 229133720.01 exhibits low levels of variability in phase with the transit signal, which could be due to ellipsoidal variations; thus we do not validate the candidate in spite of its low FPP. Subsequent analysis of the candidate 201390048.01 revealed marginal evidence of odd-even varations of transit depth, which could be an indication that the signal is actually caused by a system of two eclipsing luminous bodies at twice the estimated orbital period. Although `vespa` accounts for this scenario in its FPP calculation, we do not validate the candidate even though its FPP is below 1%. We note, however, that further observations would shed light on the true nature of this candidate, either by measuring RV variations with precision spectrographs or via simultaneous multi-band transit observations with instruments such as MuSCAT (Narita et al. 2015) and MuSCAT2 (a *griz* clone of MuSCAT now in operation at Teide Observatory).

The candidates 228974907.01, 201128338.01, and 228846243.01 all have relatively long orbital periods and thus transit only twice within the ∼80 day observing window of *K2* campaign 10. None of them have

[4] https://exoplanetarchive.ipac.caltech.edu/

particularly low FPPs or high SNR, but they may be worthy of further follow-up observations.

The integrated FPP of the full set of candidates is ∼2%, which implies the existence of 1–2 false positives among these 26 unvalidated candidates. We have already confirmed that 228729473.01 is a false positive (see Csizmadia et al., in prep.), and we suspect both 229133720.01 and 201390048.01 of also being false positives. Therefore, we expect there to be no remaining false positives, either in the set of validated planets or the remaining unvalidated candidates, and most of these should be easily validated via future observations.

6. DISCUSSION

6.1. *Interesting new systems*

6.1.1. *Ultra-short period planets*

Ultra-short period planets (USPs) are defined by having orbital periods less than one day (e.g. Sanchis-Ojeda et al. 2013, 2015). We present four validated USPs from *K2* C10, three of which have not previously been reported in the literature. Dai et al. (2017) reported the discovery and characterization of the USP K2-131b = EPIC-228732031b, and we confirm this discovery in this work. The three new USPs we report here are EPIC-201110617b ($P_{\rm orb} = 0.813137^{+0.000076}_{-0.000079}$ d), EPIC-228721452b ($P_{\rm orb} = 0.505644^{+0.000056}_{-0.000054}$ d), and EPIC-228801451b ($P_{\rm orb} = 0.584259^{+0.000017}_{-0.000017}$ d). These discoveries join a growing list of USPs discovered by *K2* (e.g. Vanderburg et al. 2016c; Christiansen et al. 2017; Gandolfi et al. 2017; Adams et al. 2017; Dai et al. 2017; Barragán et al. 2017b; Malavolta et al. 2018). The radii of these USPs place all three of them below the recently observed gap in the radius distribution (Fulton et al. 2017; Van Eylen et al. 2017) which was predicted as a consequence of photoevaporation (e.g. Owen & Wu 2013; Lopez & Fortney 2014). These three USPs are therefore likely to be rocky and have high densities, consistent with having lost any primordial or secondary atmospheres they might once have had. Of these three newly validated USPs, we measured the metallicity of the host stars spectroscopically for two of them; EPIC-228801451 appears to have only a modestly sub-solar metallitic of -0.08 ± 0.02 [Fe/H], but EPIC-201110617 has a significantly sub-solar metallicity of -0.44 ± 0.08 [Fe/H] (see Table 7). Due to their small size, these USPs are likely to have a mass less than 5 $M_\oplus$, and thus the sub-solar metallicity of their host stars would be consistent with the USP mass-metallicity trend noted by Sinukoff et al. (2017) (i.e. similar to Kepler-78b and Kepler-10b).

EPIC-228721452b and EPIC-228801451b have relatively bright host stars, as well as predicted masses and Doppler semi-amplitudes well within the reach of current precision spectrographs, such as HARPS or HIRES. EPIC-201110617b orbits a slightly fainter star and has a slightly smaller predicted mass and Doppler semi-amplitude, but is also a viable target for characterization with today's instrumentation. Such mass measurements would yield densities and constrain the bulk compositions of these USPs, which would enable tests of USP formation theories.

In addition to the four validated USPs mentioned above, we also note that our sample contains two USP candidates: 201595106.01 and 228836835.01. We do not validate 201595106.01 because of the presence of a faint star in the EPIC with a ΔK_p of 5.839 and a separation of 13.62″(see Table 3), which is within the photometric aperture we used to extract the *K2* light curve. We do not validate 228836835.01 because it has a FPP of 7.6% and thus does not meet our validation criterion. Future observations could potentially rule out false positive scenarios for both of these candidates, resulting in the validation of two more USPs from *K2* C10.

6.1.2. *Multi-planet systems*

Of the 45 validated planets in our sample, 18 of them were found in two-planet systems, which enables the study of their orbital architectures and evolution. Four of these systems have orbital architectures with period ratios just wide of a 2:1 first-order mean motion resonance (MMR), and two are close to a 3:1 second-order MMR. The pairs closest to 2:1 MMR are EPIC-201166680bc and EPIC-228934525bc, which both have $P_c/P_b \approx 2.16$. The relatively large fraction of multi-planet systems (4/9) in our sample with period ratios just wide of a 2:1 MMR is reminiscent of the distribution of orbital architectures observed with *Kepler* (Fabrycky et al. 2014). EPIC-228849382bc and EPIC-228725791bc are both just inside the 3:1 second-order MMR, with period ratios of $P_c/P_b \approx 2.96$ and $P_c/P_b \approx 2.89$, respectively. Although we did not detect any significant TTVs in the *K2* data, some of these systems may have TTVs which could be detected with higher cadence transit observations.

Intriguingly, two of the four validated USPs in the sample were found in two-planet systems with large period ratios: EPIC-228721452bc has $P_c/P_b \approx 9.02$, and EPIC-228801451bc has $P_c/P_b \approx 14.25$. The presence of an additional transiting planet decreases the likelihood that these USPs reached their current orbits via dynamical scattering, as this would increase the chances of higher eccentricities; even after tidal circularization, the geometric transit probability would be decreased by a higher likelihood of non-coplanarity. This is consistent

with previous analyses in which USP systems have been noted to be dynamically cold (e.g. Dai et al. 2017).

6.1.3. *EPIC-228974324*

At first glance, EPIC-228974324b appears to be a Mars-size planet orbiting an early M dwarf in the local bubble. However, this estimate of the planet radius is dependent on the host star's radius estimated by H16 ($R_\star = 0.281 \pm 0.015\ R_\odot$). Based on optical/near-IR colors and Monte Carlo interpolation of the table of Pecaut & Mamajek (2013)[5], EPIC-228974324 has spectral type SpT $\approx M1 \pm 1$, $d_{\rm phot} \sim 60$ pc, and $M_\star \sim 0.5\ M_\odot$. These estimates are consistent with the mean stellar density we measure from the light curve $\rho_{\star,LC} = 2.82^{+1.26}_{-1.57}\rho_\odot$. Furthermore, Dressing et al. (2017b) found that H16 typically understimated M dwarf radii by ∼40% due to a systematic effect arising from the isochrones underlying the analysis. We conclude that the host star's radius is likely underestimated by H16, and that the planet is therefore likely to be closer to Earth in size. This also implies a larger predected mass and Doppler semi-amplitude than we list in Table 6, which means the planet could be a viable target for characterization via mass measurement. Such a measurement would yield the planet's density and constrain its composition, and would also help improve our knowledge of the mass-radius relation for planets in the terrestrial size regime.

6.2. *Characterization targets*

We predicted the masses of the candidates using the probabilistic mass-radius relation of Wolfgang et al. (2016)[6] (see Table 6). The predicted masses enabled us to compute other quanitities of interest, which we then used to identify potentially interesting targets for follow-up characterization via Doppler and transmission spectroscopy.

6.2.1. *Doppler targets*

We computed the expected Doppler semi-amplitude due to the reflex motion of the host star induced by each planet (see Table 6). We used these expected semi-amplitudes in conjunction with the brightness of the host stars to identify planets in the sample which are good targets for radial velocity (RV) follow-up study using current and future facilities. Such RV observations will reveal the planets' densities and constrain their bulk compositions. This is of particular interest for relatively small planets with radii in the range $1.5 - 2.5\ R_\oplus$ because such measurements could enable tests of planet formation theories and post-processes, such as the photoevaporation (e.g. Owen & Wu 2013; Lopez & Fortney 2014), which has been proposed to explain the observed gap in the radius distribution (Fulton et al. 2017; Van Eylen et al. 2017). However, because of the difficulty of detecting the small Doppler signals of such planets, it is especially important to identify such planets which are orbiting relatively bright stars, for which the RV precision required to measure their masses is more readily obtainable. Table 4 lists validated planets with predicted Doppler semi-amplitudes greater than 1 m s^{-1} orbiting stars brighter than $K_p = 12$ mag. For convenience, we also list planetary orbital periods and stellar rotational periods (when available); potentially confounding quasi-periodic RV signals produced by stellar magnetic activity are less likely to present a challenge for mass measurement when the orbital period is far from the stellar rotational period (or a harmonic).

Table 4. Validated planets with predicted Doppler semi-amplitudes greater than 1 m s^{-1} orbiting stars brighter than $K_p = 12$ mag.

EPIC	K_p [mag]	$K_{\rm pred}$ [m s^{-1}]	R_P [$R_\oplus$]	P [days]	$P_{\rm rot}$ [days]
201092629.01	11.858	$2.1^{+0.6}_{-0.6}$	2.27	26.8198	22^{+6}_{-2}
201111557.01	11.363	$1.1^{+0.9}_{-0.7}$	1.06	2.3018	12.0±1.8
201132684.01	11.678	$1.0^{+0.8}_{-0.6}$	1.18	5.9028	13.8±1.3
201132684.02	11.678	$2.7^{+0.8}_{-0.8}$	2.46	10.0605	13.8±1.3
201164625.01	11.919	$2.8^{+1.6}_{-1.5}$	2.15	2.7118	12.5±1.5
201166680.01	10.897	$1.8^{+0.7}_{-0.6}$	2.18	11.5420	—
201166680.02	10.897	$1.3^{+0.5}_{-0.5}$	2.07	24.9454	—
201211526.01	11.696	$1.3^{+0.6}_{-0.6}$	1.62	21.0687	—
201225286.01	11.729	$2.4^{+0.8}_{-0.8}$	2.14	12.4220	20.8±1.6
201357643.01	11.998	$6.9^{+2.7}_{-2.0}$	5.36	11.8930	—
201437844.01	9.234	$2.4^{+0.7}_{-0.7}$	2.31	9.5580	—
201437844.02	9.234	$4.0^{+0.9}_{-0.8}$	4.28	21.0578	—
201595106.01	11.678	$1.9^{+1.2}_{-1.0}$	1.19	0.8770	—
201615463.01	11.964	$2.5^{+0.9}_{-0.9}$	2.51	8.5282	—
228721452.01	11.325	$2.6^{+2.7}_{-2.2}$	1.39	0.5056	—
228721452.02	11.325	$2.9^{+1.7}_{-1.6}$	2.44	4.5633	—
228732031.01	11.937	$5.8^{+2.3}_{-2.2}$	1.84	0.3693	9.4±1.9
228734900.01	11.535	$3.6^{+1.2}_{-1.0}$	3.93	15.8720	—
228801451.01	10.955	$2.3^{+1.1}_{-1.3}$	1.16	0.5843	19.5±2.7
228801451.02	10.955	$2.4^{+0.8}_{-0.8}$	2.07	8.3273	19.5±2.7

6.2.2. *Atmospheric targets*

In order to identify viable new targets for atmospheric studies via transmission spectroscopy, we used the properties of the host stars and planets to predict atmospheric scale heights and the amplitudes of the wavelength dependence of transit depth ($\delta_{\rm TS}$). Following Miller-Ricci et al. (2009), we calculated the atmospheric

[5] https://github.com/john-livingston/hoshi
[6] https://github.com/john-livingston/wolfie

Table 5. Predicted atmospheric characteristics, where g is surface gravity, H is atmospheric scale height, and $\delta_{\rm TS}$ is the expected amplitude of wavelength-dependent atmospheric features which could be observed via transmission spectroscopy.

EPIC	J [mag]	g [$g_\oplus$]	H [km]	$\delta_{\rm TS}$ [ppm]
228735255.01	11.421	0.45	892	1465
228894622.01	11.556	1.29	329	278
228974324.01	10.477	0.39	688	551

scale height H and $\delta_{\rm TS}$ for each validated planet by

$$H = \frac{29.26}{(\mu/28.96)} \frac{T_{\rm eq}}{g} \quad [\rm m] \tag{2}$$

$$\delta_{\rm TS} \sim 10\, H \cdot R_P/R_\star^2, \tag{3}$$

where μ, $T_{\rm eq}$, and g are the mean molecular weight, planet equilibrium temperature, and planet surface gravity, respectively. We used the predicted planet mass estimated in Section 6.2 to predict the surface gravity, and assumed a bond albedo of 0.3 and a mean molecular weight $\mu = 2$ (hydrogen-dominated atmosphere) for each planet (see Table 11). We note that this assumption for μ is likely to be invalid for the smaller planets in our sample (i.e. $R_P \lesssim 1.5$–$2\ R_\oplus$), as they are not likely to have substantial hydrogen-dominated atmospheres; these smaller planets likely have higher mean molecular weight atmospheres, which would make their characterization via transmission spectroscopy more challenging. Table 5 lists planets with relatively bright host stars ($J < 12$ mag) and large expected transmission spectroscopy signals ($\delta_{\rm TS} > 200$ ppm).

7. SUMMARY

We detected 72 planet candidates in *K2* campaign 10 and obtained high resolution imaging and spectroscopy follow-up observations to characterize the host stars. We performed detailed modeling of the light curves and used the resulting transit parameters to compute physical planet properties. We used the planet and host star properties to predict masses and atmospheric signals, which enabled us to identify good targets for future characterization via Doppler and transmission spectroscopy. We statistically validated 45 planets, leaving a remainder of 26 candidates one false positive. We expect nearly all of these remaining candidates to be real planets, which could potentially be validated via further observations and analysis.

This work was carried out as part of the KESPRINT consortium. The WIYN/NESSI observations were conducted as part of an approved NOAO observing program (P.I. Livingston, proposal ID 2017A-0377). Data presented herein were obtained at the WIYN Observatory from telescope time allocated to NN-EXPLORE through the scientific partnership of the National Aeronautics and Space Administration, the National Science Foundation, and the National Optical Astronomy Observatory. This work was supported by a NASA WIYN PI Data Award, administered by the NASA Exoplanet Science Institute. NESSI was funded by the NASA Exoplanet Exploration Program and the NASA Ames Research Center. NESSI was built at the Ames Research Center by Steve B. Howell, Nic Scott, Elliott P. Horch, and Emmett Quigley. The authors are honored to be permitted to conduct observations on Iolkam Du'ag (Kitt Peak), a mountain within the Tohono O'odham Nation with particular significance to the Tohono O'odham people. J. H. L. gratefully acknowledges the support of the Japan Society for the Promotion of Science (JSPS) Research Fellowship for Young Scientists. M.E. and W.D.C. were supported by NASA grant NNX16AJ11G to The University of Texas. This paper includes data collected by the *Kepler* mission. Funding for the *Kepler* mission is provided by the NASA Science Mission directorate.

Facilities: Kepler, WIYN (NESSI), McDonald (Tull), NOT (FIES), TNG (HARPS-N)

Software: `scipy`, `emcee`, `batman`, `vespa`, `IRAF`

REFERENCES

Adams, E. R., Jackson, B., Endl, M., et al. 2017, AJ, 153, 82

Akeson, R. L., Chen, X., Ciardi, D., et al. 2013, PASP, 125, 989

Barragán, O., & Gandolfi, D. 2017, Exotrending: Fast and easy-to-use light curve detrending software for exoplanets, Astrophysics Source Code Library, , , ascl:1706.001

Barragán, O., Gandolfi, D., & Antoniciello, G. 2017a, pyaneti: Multi-planet radial velocity and transit fitting, Astrophysics Source Code Library, , , ascl:1707.003

Barragán, O., Gandolfi, D., Dai, F., et al. 2017b, ArXiv e-prints, arXiv:1711.02097

Cabrera, J., Csizmadia, S., Erikson, A., Rauer, H., & Kirste, S. 2012, A&A, 548, A44

Christiansen, J. L., Vanderburg, A., Burt, J., et al. 2017, AJ, 154, 122

Ciardi, D. R., Crossfield, I. J. M., Feinstein, A. D., et al. 2017, ArXiv e-prints, arXiv:1709.10398

Claret, A., Hauschildt, P. H., & Witte, S. 2012, VizieR Online Data Catalog, 354

Cosentino, R., Lovis, C., Pepe, F., et al. 2012, in Proc. SPIE, Vol. 8446, Ground-based and Airborne Instrumentation for Astronomy IV, 84461V

Crossfield, I. J. M., Petigura, E., Schlieder, J. E., et al. 2015, ApJ, 804, 10

Crossfield, I. J. M., Ciardi, D. R., Petigura, E. A., et al. 2016, ApJS, 226, 7

Crossfield, I. J. M., Ciardi, D. R., Isaacson, H., et al. 2017, AJ, 153, 255

Dai, F., Winn, J. N., Gandolfi, D., et al. 2017, AJ, 154, 226

David, T. J., Hillenbrand, L. A., Petigura, E. A., et al. 2016a, Nature, 534, 658

David, T. J., Conroy, K. E., Hillenbrand, L. A., et al. 2016b, AJ, 151, 112

Dotter, A., Chaboyer, B., Jevremović, D., et al. 2008, ApJS, 178, 89

Dressing, C. D., Newton, E. R., Schlieder, J. E., et al. 2017a, ArXiv e-prints, arXiv:1701.00586

Dressing, C. D., Vanderburg, A., Schlieder, J. E., et al. 2017b, AJ, 154, 207

Endl, M., & Cochran, W. D. 2016, PASP, 128, 094502

Fabrycky, D. C., Lissauer, J. J., Ragozzine, D., et al. 2014, ApJ, 790, 146

Feroz, F., Hobson, M. P., Cameron, E., & Pettitt, A. N. 2013, ArXiv e-prints, arXiv:1306.2144

Foreman-Mackey, D., Hogg, D. W., Lang, D., & Goodman, J. 2013, PASP, 125, 306

Frandsen, S., & Lindberg, B. 1999, in Astrophysics with the NOT, ed. H. Karttunen & V. Piirola, 71

Fridlund, M., Gaidos, E., Barragán, O., et al. 2017, A&A, 604, A16

Fulton, B. J., Petigura, E. A., Howard, A. W., et al. 2017, AJ, 154, 109

Gaidos, E., Mann, A. W., Rizzuto, A., et al. 2017, MNRAS, 464, 850

Gandolfi, D., Parviainen, H., Fridlund, M., et al. 2013, A&A, 557, A74

Gandolfi, D., Barragán, O., Hatzes, A. P., et al. 2017, AJ, 154, 123

Giles, H. A. C., Bayliss, D., Espinoza, N., et al. 2017, ArXiv e-prints, arXiv:1706.06865

Girardi, L., Groenewegen, M. A. T., Hatziminaoglou, E., & da Costa, L. 2005, A&A, 436, 895

Goodman, J., & Weare, J. 2010, Communications in Applied Mathematics and Computational Science, Vol. 5, No. 1, p. 65-80, 2010, 5, 65

Grziwa, S., & Pätzold, M. 2016, ArXiv e-prints, arXiv:1607.08417

Guenther, E. W., Barragan, O., Dai, F., et al. 2017, ArXiv e-prints, arXiv:1705.04163

Hirano, T., Dai, F., Gandolfi, D., et al. 2017, ArXiv e-prints, arXiv:1710.03239

Horch, E. P., Howell, S. B., Everett, M. E., & Ciardi, D. R. 2012, AJ, 144, 165

Horch, E. P., Veillette, D. R., Baena Gallé, R., et al. 2009, AJ, 137, 5057

Horch, E. P., Casetti-Dinescu, D. I., Camarata, M. A., et al. 2017, AJ, 153, 212

Howell, S. B., Everett, M. E., Sherry, W., Horch, E., & Ciardi, D. R. 2011, AJ, 142, 19

Howell, S. B., Sobeck, C., Haas, M., et al. 2014, PASP, 126, 398

Huber, D., Bryson, S. T., Haas, M. R., et al. 2016, ApJS, 224, 2

Jones, E., Oliphant, T., Peterson, P., et al. 2001–present, SciPy: Open source scientific tools for Python, ,

Kipping, D. M. 2010, MNRAS, 408, 1758

Kovács, G., Zucker, S., & Mazeh, T. 2002, A&A, 391, 369

Kreidberg, L. 2015, PASP, 127, 1161

Lissauer, J. J., Ragozzine, D., Fabrycky, D. C., et al. 2011, ApJS, 197, 8

Lissauer, J. J., Marcy, G. W., Rowe, J. F., et al. 2012, ApJ, 750, 112

Lissauer, J. J., Marcy, G. W., Bryson, S. T., et al. 2014, ApJ, 784, 44

Livingston, J. H., Dai, F., Hirano, T., et al. 2017, ArXiv e-prints, arXiv:1710.07203

Lohmann, A. W., Weigelt, G., & Wirnitzer, B. 1983, ApOpt, 22, 4028

Lomb, N. R. 1976, Ap&SS, 39, 447

Lopez, E. D., & Fortney, J. J. 2014, ApJ, 792, 1

Malavolta, L., Mayo, A. W., Louden, T., et al. 2018, ArXiv e-prints, arXiv:1801.03502

Mandel, K., & Agol, E. 2002, ApJL, 580, L171

Mann, A. W., Gaidos, E., Mace, G. N., et al. 2016a, ApJ, 818, 46

Mann, A. W., Newton, E. R., Rizzuto, A. C., et al. 2016b, AJ, 152, 61

Mann, A. W., Gaidos, E., Vanderburg, A., et al. 2017a, AJ, 153, 64

Mann, A. W., Vanderburg, A., Rizzuto, A. C., et al. 2017b, ArXiv e-prints, arXiv:1709.10328

McQuillan, A., Mazeh, T., & Aigrain, S. 2014, ApJS, 211, 24

Miller-Ricci, E., Seager, S., & Sasselov, D. 2009, ApJ, 690, 1056

Montet, B. T., Morton, T. D., Foreman-Mackey, D., et al. 2015, ApJ, 809, 25

Morton, T. D. 2012, ApJ, 761, 6

—. 2015a, isochrones: Stellar model grid package, Astrophysics Source Code Library, , , ascl:1503.010

—. 2015b, VESPA: False positive probabilities calculator, Astrophysics Source Code Library, , , ascl:1503.011

Morton, T. D., Bryson, S. T., Coughlin, J. L., et al. 2016, ApJ, 822, 86

Narita, N., Fukui, A., Kusakabe, N., et al. 2015, Journal of Astronomical Telescopes, Instruments, and Systems, 1, 045001

Newville, M., Stensitzki, T., Allen, D. B., & Ingargiola, A. 2014, LMFIT: Non-Linear Least-Square Minimization and Curve-Fitting for Python¶, , , doi:10.5281/zenodo.11813

Niraula, P., Redfield, S., Dai, F., et al. 2017, AJ, 154, 266

Obermeier, C., Henning, T., Schlieder, J. E., et al. 2016, AJ, 152, 223

Ofir, A. 2014, A&A, 561, A138

Owen, J. E., & Wu, Y. 2013, ApJ, 775, 105

Pecaut, M. J., & Mamajek, E. E. 2013, ApJS, 208, 9

Pepper, J., Gillen, E., Parviainen, H., et al. 2017, AJ, 153, 177

Petigura, E. A., Schlieder, J. E., Crossfield, I. J. M., et al. 2015, ApJ, 811, 102

Rodriguez, J. E., Zhou, G., Vanderburg, A., et al. 2017, AJ, 153, 256

Sanchis-Ojeda, R., Rappaport, S., Winn, J. N., et al. 2013, ApJ, 774, 54

Sanchis-Ojeda, R., Rappaport, S., Pallè, E., et al. 2015, ApJ, 812, 112

Scargle, J. D. 1982, ApJ, 263, 835

Scott, N. J., Howell, S. B., & Horch, E. P. 2016, in Proc. SPIE, Vol. 9907, Optical and Infrared Interferometry and Imaging V, 99072R

Sinukoff, E., Howard, A. W., Petigura, E. A., et al. 2016, ApJ, 827, 78

—. 2017, AJ, 153, 271

Smith, A. M. S., Cabrera, J., Csizmadia, S., et al. 2018, MNRAS, 474, 5523

Telting, J. H., Avila, G., Buchhave, L., et al. 2014, Astronomische Nachrichten, 335, 41

Tull, R. G., MacQueen, P. J., Sneden, C., & Lambert, D. L. 1995, PASP, 107, 251

Van Eylen, V., Agentoft, C., Lundkvist, M. S., et al. 2017, ArXiv e-prints, arXiv:1710.05398

Vanderburg, A., & Johnson, J. A. 2014, PASP, 126, 948

Vanderburg, A., Montet, B. T., Johnson, J. A., et al. 2015, ApJ, 800, 59

Vanderburg, A., Becker, J. C., Kristiansen, M. H., et al. 2016a, ApJL, 827, L10

Vanderburg, A., Latham, D. W., Buchhave, L. A., et al. 2016b, ApJS, 222, 14

Vanderburg, A., Bieryla, A., Duev, D. A., et al. 2016c, ApJL, 829, L9

Wolfgang, A., Rogers, L. A., & Ford, E. B. 2016, ApJ, 825, 19

Yee, S. W., Petigura, E. A., & von Braun, K. 2017, ApJ, 836, 77

Table 6. Planet candidate parameters.

EPIC	$P_{\rm orb}$ [days]	T_0 [BKJD]	a [$R_\star$]	R_P [$R_\star$]	a [AU]	R_P [$R_\oplus$]	$T_{\rm eq}$ [K]	M_P [$M_\oplus$]	$K_{\rm pred}$ [m s^{-1}]	$\rho_{\star,LC}$ [$\rho_\odot$]	FPP	Disposition
201092629.01	$26.819836^{+0.002407}_{-0.002424}$	$2751.20638^{+0.00344}_{-0.00326}$	$44.2^{+3.2}_{-8.3}$	$0.0309^{+0.0017}_{-0.0010}$	$0.1561^{+0.0015}_{-0.0016}$	$2.27^{+0.14}_{-0.10}$	467^{+10}_{-10}	$7.8^{+2.4}_{-2.3}$	$2.1^{+0.6}_{-0.6}$	$1.61^{+0.38}_{-0.75}$	3.6×10^{-7}	Planet
201102594.01	$6.513853^{+0.000836}_{-0.000850}$	$2753.23997^{+0.00533}_{-0.00515}$	$22.0^{+3.9}_{-5.7}$	$0.0635^{+0.0052}_{-0.0044}$	$0.0477^{+0.0027}_{-0.0031}$	$2.19^{+0.40}_{-0.37}$	423^{+38}_{-38}	$7.5^{+2.9}_{-2.8}$	$5.2^{+2.2}_{-2.0}$	$3.37^{+2.11}_{-1.99}$	4.0×10^{-10}	Planet
201110617.01	$0.813137^{+0.000076}_{-0.000079}$	$2750.14285^{+0.00410}_{-0.00394}$	$4.1^{+0.6}_{-0.9}$	$0.0161^{+0.0015}_{-0.0010}$	$0.0146^{+0.0002}_{-0.0002}$	$1.06^{+0.10}_{-0.07}$	1269^{+27}_{-26}	$1.9^{+1.3}_{-1.1}$	$1.8^{+1.2}_{-1.1}$	$1.44^{+0.75}_{-0.74}$	3.9×10^{-10}	Planet
201111557.01	$2.301838^{+0.000284}_{-0.000290}$	$2750.16855^{+0.00521}_{-0.00508}$	$11.6^{+2.0}_{-2.9}$	$0.0145^{+0.0014}_{-0.0010}$	$0.0308^{+0.0007}_{-0.0007}$	$1.06^{+0.13}_{-0.10}$	947^{+47}_{-46}	$1.8^{+1.5}_{-1.1}$	$1.1^{+0.9}_{-0.6}$	$3.93^{+2.46}_{-2.27}$	8.3×10^{-5}	Candidate
201127519.01	$6.178882^{+0.000071}_{-0.000081}$	$2752.54725^{+0.00057}_{-0.00053}$	$17.7^{+0.4}_{-0.8}$	$0.1064^{+0.0015}_{-0.0009}$	$0.0611^{+0.0006}_{-0.0007}$	$8.70^{+0.25}_{-0.24}$	757^{+14}_{-15}	$43.1^{+16.0}_{-11.5}$	$17.5^{+6.6}_{-4.7}$	$1.96^{+0.15}_{-0.24}$	2.0×10^{-2}	Candidate
201128338.01	$32.643661^{+0.013884}_{-0.020699}$	$2775.62505^{+0.01957}_{-0.00898}$	$52.7^{+9.3}_{-13.1}$	$0.0349^{+0.0049}_{-0.0041}$	$0.1635^{+0.0030}_{-0.0030}$	$2.03^{+0.31}_{-0.27}$	340^{+15}_{-14}	$6.8^{+2.8}_{-2.7}$	$2.0^{+0.8}_{-0.8}$	$1.85^{+1.16}_{-1.06}$	1.0×10^{-2}	Candidate
201132684.01	$5.902811^{+0.001902}_{-0.002329}$	$2750.88310^{+0.01321}_{-0.01186}$	$11.3^{+2.4}_{-2.9}$	$0.0124^{+0.0011}_{-0.0010}$	$0.0618^{+0.0018}_{-0.0019}$	$1.18^{+0.14}_{-0.13}$	921^{+41}_{-40}	$2.7^{+2.0}_{-1.6}$	$1.0^{+0.7}_{-0.6}$	$0.56^{+0.45}_{-0.33}$	1.8×10^{-9}	Planet
201132684.02	$10.060528^{+0.001315}_{-0.001579}$	$2757.48332^{+0.00814}_{-0.00633}$	$19.0^{+1.7}_{-4.2}$	$0.0256^{+0.0016}_{-0.0008}$	$0.0881^{+0.0026}_{-0.0027}$	$2.46^{+0.24}_{-0.21}$	771^{+34}_{-34}	$8.6^{+2.6}_{-2.5}$	$2.7^{+0.9}_{-0.8}$	$0.91^{+0.26}_{-0.48}$	9.2×10^{-9}	Planet
201164625.01	$2.711844^{+0.000688}_{-0.000568}$	$2750.13703^{+0.01072}_{-0.01786}$	$5.6^{+1.0}_{-1.5}$	$0.0120^{+0.0010}_{-0.0008}$	$0.0414^{+0.0016}_{-0.0017}$	$2.16^{+0.73}_{-0.70}$	1712^{+258}_{-300}	$7.4^{+4.0}_{-4.0}$	$2.8^{+1.6}_{-1.5}$	$0.32^{+0.21}_{-0.19}$	9.0×10^{-4}	Candidate
201166680.01	$11.541993^{+0.002712}_{-0.002395}$	$2760.20557^{+0.00864}_{-0.01034}$	$21.2^{+2.1}_{-5.1}$	$0.0143^{+0.0009}_{-0.0007}$	$0.1089^{+0.0035}_{-0.0038}$	$2.18^{+0.28}_{-0.27}$	1058^{+65}_{-66}	$7.4^{+2.6}_{-2.6}$	$1.8^{+0.7}_{-0.6}$	$0.96^{+0.31}_{-0.53}$	6.7×10^{-5}	Planet
201166680.02	$24.945382^{+0.004959}_{-0.005368}$	$2751.50541^{+0.00746}_{-0.00709}$	$35.0^{+4.0}_{-9.0}$	$0.0136^{+0.0010}_{-0.0009}$	$0.1820^{+0.0058}_{-0.0063}$	$2.07^{+0.29}_{-0.26}$	819^{+50}_{-52}	$6.9^{+2.6}_{-2.5}$	$1.3^{+0.5}_{-0.5}$	$0.93^{+0.36}_{-0.55}$	1.3×10^{-4}	Planet
201180665.01	$17.772975^{+0.000104}_{-0.000093}$	$2753.49856^{+0.00021}_{-0.00022}$	$33.4^{+0.4}_{-0.4}$	$0.1890^{+0.0009}_{-0.0011}$	$0.1302^{+0.0041}_{-0.0046}$	$21.83^{+5.88}_{-5.66}$	747^{+97}_{-109}	$134.2^{+128.3}_{-63.6}$	$34.6^{+33.1}_{-16.6}$	$1.58^{+0.06}_{-0.05}$	2.1×10^{-1}	Candidate
201211526.01	$21.068708^{+0.003200}_{-0.003121}$	$2755.47492^{+0.00611}_{-0.00654}$	$38.6^{+5.5}_{-10.0}$	$0.0174^{+0.0012}_{-0.0009}$	$0.1426^{+0.0012}_{-0.0012}$	$1.62^{+0.16}_{-0.14}$	610^{+22}_{-22}	$5.2^{+2.3}_{-2.3}$	$1.3^{+0.6}_{-0.6}$	$1.74^{+0.85}_{-1.03}$	2.1×10^{-3}	Planet
201225286.01	$12.422028^{+0.001770}_{-0.001876}$	$2753.50783^{+0.00774}_{-0.00766}$	$28.1^{+4.1}_{-8.1}$	$0.0250^{+0.0021}_{-0.0012}$	$0.0968^{+0.0025}_{-0.0027}$	$2.14^{+0.22}_{-0.18}$	693^{+28}_{-28}	$7.3^{+2.5}_{-2.4}$	$2.4^{+0.8}_{-0.8}$	$1.93^{+0.96}_{-1.24}$	1.9×10^{-5}	Planet
201274010.01	$13.011044^{+0.005004}_{-0.003993}$	$2756.51502^{+0.00851}_{-0.01168}$	$26.2^{+5.8}_{-7.7}$	$0.0257^{+0.0030}_{-0.0025}$	$0.1058^{+0.0030}_{-0.0032}$	$2.62^{+0.64}_{-0.57}$	743^{+71}_{-78}	$9.4^{+3.9}_{-3.6}$	$2.7^{+1.1}_{-1.0}$	$1.42^{+1.18}_{-0.92}$	1.6×10^{-1}	Candidate
201352100.01	$13.383929^{+0.001069}_{-0.001156}$	$2761.78914^{+0.00329}_{-0.00312}$	$34.3^{+2.5}_{-6.8}$	$0.0326^{+0.0019}_{-0.0010}$	$0.1052^{+0.0009}_{-0.0009}$	$2.84^{+0.18}_{-0.12}$	636^{+12}_{-12}	$10.5^{+2.5}_{-2.5}$	$3.1^{+0.7}_{-0.8}$	$3.01^{+0.72}_{-1.46}$	3.5×10^{-5}	Candidate
201357643.01	$11.893035^{+0.000622}_{-0.000650}$	$2754.55245^{+0.00179}_{-0.00167}$	$17.2^{+1.4}_{-2.5}$	$0.0318^{+0.0011}_{-0.0006}$	$0.0973^{+0.0023}_{-0.0022}$	$5.33^{+1.16}_{-1.10}$	990^{+101}_{-108}	$22.7^{+9.3}_{-6.9}$	$7.0^{+2.8}_{-2.1}$	$0.48^{+0.13}_{-0.18}$	1.3×10^{-10}	Planet
201386739.01	$5.769192^{+0.000814}_{-0.000845}$	$2750.67605^{+0.00652}_{-0.00612}$	$11.1^{+1.1}_{-2.4}$	$0.0341^{+0.0022}_{-0.0017}$	$0.0601^{+0.0004}_{-0.0004}$	$3.50^{+0.36}_{-0.32}$	976^{+37}_{-38}	$13.5^{+3.3}_{-3.1}$	$5.3^{+1.3}_{-1.2}$	$0.55^{+0.18}_{-0.28}$	9.8×10^{-5}	Planet
201390048.01	$9.458811^{+0.001013}_{-0.001002}$	$2750.90793^{+0.00460}_{-0.00425}$	$23.2^{+2.5}_{-5.3}$	$0.0191^{+0.0016}_{-0.0010}$	$0.0794^{+0.0019}_{-0.0019}$	$1.43^{+0.15}_{-0.12}$	610^{+24}_{-25}	$4.4^{+2.3}_{-2.1}$	$1.6^{+0.8}_{-0.8}$	$1.88^{+0.66}_{-1.02}$	2.3×10^{-3}	Candidate
201390927.01	$2.638000^{+0.000278}_{-0.000278}$	$2750.34092^{+0.00432}_{-0.00438}$	$11.0^{+1.7}_{-2.4}$	$0.0262^{+0.0022}_{-0.0018}$	$0.0312^{+0.0006}_{-0.0006}$	$1.51^{+0.16}_{-0.14}$	754^{+27}_{-27}	$4.7^{+2.4}_{-2.3}$	$3.1^{+1.6}_{-1.5}$	$2.54^{+1.38}_{-1.34}$	1.7×10^{-8}	Candidate
201392505.01	$27.472533^{+0.010433}_{-0.014328}$	$2759.07732^{+0.02075}_{-0.01599}$	$31.4^{+2.9}_{-6.4}$	$0.0410^{+0.0028}_{-0.0019}$	$0.1648^{+0.0017}_{-0.0018}$	$3.29^{+0.24}_{-0.19}$	475^{+9}_{-9}	$12.5^{+2.8}_{-2.7}$	$3.1^{+0.7}_{-0.7}$	$0.55^{+0.17}_{-0.27}$	9.7×10^{-9}	Candidate
201437844.01	$9.558024^{+0.001612}_{-0.001733}$	$2753.52675^{+0.00705}_{-0.00656}$	$17.3^{+1.9}_{-4.8}$	$0.0165^{+0.0011}_{-0.0006}$	$0.0890^{+0.0008}_{-0.0009}$	$2.31^{+0.17}_{-0.14}$	1046^{+25}_{-25}	$8.0^{+2.4}_{-2.4}$	$2.4^{+0.7}_{-0.7}$	$0.77^{+0.28}_{-0.47}$	6.7×10^{-5}	Planet
201437844.02	$21.057849^{+0.001300}_{-0.001304}$	$2757.07335^{+0.00199}_{-0.00202}$	$34.6^{+1.2}_{-3.7}$	$0.0305^{+0.0006}_{-0.0004}$	$0.1507^{+0.0014}_{-0.0015}$	$4.28^{+0.20}_{-0.19}$	804^{+19}_{-19}	$17.5^{+3.8}_{-3.4}$	$4.0^{+0.9}_{-0.8}$	$1.26^{+0.14}_{-0.36}$	6.8×10^{-6}	Planet
201595106.01	$0.877045^{+0.000111}_{-0.000125}$	$2750.05088^{+0.00495}_{-0.00475}$	$5.5^{+1.4}_{-1.3}$	$0.0114^{+0.0011}_{-0.0009}$	$0.0180^{+0.0001}_{-0.0001}$	$1.19^{+0.12}_{-0.10}$	1869^{+30}_{-30}	$2.8^{+1.8}_{-1.6}$	$1.8^{+1.2}_{-1.0}$	$2.90^{+2.73}_{-1.65}$	1.3×10^{-3}	Candidate
201598502.01	$7.515605^{+0.002036}_{-0.002455}$	$2755.42762^{+0.01370}_{-0.01101}$	$23.5^{+5.3}_{-6.3}$	$0.0346^{+0.0037}_{-0.0033}$	$0.0575^{+0.0022}_{-0.0024}$	$1.50^{+0.25}_{-0.22}$	445^{+28}_{-28}	$4.6^{+2.5}_{-2.4}$	$2.5^{+1.5}_{-1.3}$	$3.07^{+2.57}_{-1.87}$	8.6×10^{-5}	Planet
201615463.01	$8.528248^{+0.003469}_{-0.003399}$	$2753.75461^{+0.01543}_{-0.01733}$	$10.8^{+1.2}_{-2.9}$	$0.0125^{+0.0010}_{-0.0009}$	$0.0853^{+0.0029}_{-0.0031}$	$2.52^{+0.46}_{-0.42}$	1202^{+98}_{-102}	$8.9^{+3.2}_{-3.0}$	$2.5^{+0.9}_{-0.9}$	$0.23^{+0.09}_{-0.14}$	1.5×10^{-3}	Planet
228707509.01	$15.350922^{+0.000318}_{-0.000311}$	$2752.50931^{+0.00093}_{-0.00092}$	$25.3^{+1.5}_{-1.1}$	$0.1506^{+0.0025}_{-0.0034}$	$0.1130^{+0.0039}_{-0.0042}$	$12.93^{+7.18}_{-7.13}$	627^{+151}_{-183}	$69.0^{+79.3}_{-41.3}$	$20.3^{+23.6}_{-12.1}$	$0.92^{+0.18}_{-0.12}$	2.3×10^{-5}	Candidate
228720681.01	$15.781298^{+0.000383}_{-0.000383}$	$2753.41896^{+0.00098}_{-0.00099}$	$26.2^{+4.1}_{-2.5}$	$0.0981^{+0.0027}_{-0.0037}$	$0.1177^{+0.0015}_{-0.0015}$	$10.14^{+1.38}_{-1.35}$	712^{+47}_{-50}	$52.2^{+25.8}_{-16.5}$	$14.5^{+7.2}_{-4.6}$	$0.97^{+0.54}_{-0.25}$	4.8×10^{-2}	Candidate
228721452.01	$0.505644^{+0.000056}_{-0.000054}$	$2750.56405^{+0.00435}_{-0.00476}$	$3.9^{+1.1}_{-0.9}$	$0.0083^{+0.0009}_{-0.0007}$	$0.0132^{+0.0006}_{-0.0006}$	$1.39^{+0.56}_{-0.50}$	2845^{+479}_{-554}	$3.7^{+3.7}_{-3.1}$	$2.6^{+2.7}_{-2.1}$	$3.09^{+3.61}_{-1.75}$	2.2×10^{-4}	Planet
228721452.02	$4.563250^{+0.000492}_{-0.000483}$	$2749.97536^{+0.00412}_{-0.00425}$	$11.0^{+1.2}_{-2.8}$	$0.0146^{+0.0010}_{-0.0006}$	$0.0571^{+0.0025}_{-0.0027}$	$2.43^{+0.89}_{-0.86}$	1365^{+230}_{-265}	$8.5^{+4.8}_{-4.4}$	$2.9^{+1.7}_{-1.5}$	$0.86^{+0.31}_{-0.51}$	1.2×10^{-4}	Planet
228724899.01	$5.202562^{+0.000431}_{-0.000448}$	$2753.45607^{+0.00362}_{-0.00351}$	$26.8^{+3.2}_{-5.7}$	$0.0337^{+0.0023}_{-0.0017}$	$0.0580^{+0.0005}_{-0.0005}$	$3.31^{+0.27}_{-0.22}$	957^{+24}_{-24}	$12.7^{+3.0}_{-2.8}$	$4.8^{+1.2}_{-1.1}$	$9.53^{+3.77}_{-4.90}$	1.4×10^{-1}	Candidate
228725791.01	$2.250244^{+0.000308}_{-0.000355}$	$2749.97676^{+0.00622}_{-0.00577}$	$8.6^{+1.6}_{-2.3}$	$0.0284^{+0.0023}_{-0.0020}$	$0.0255^{+0.0013}_{-0.0014}$	$1.20^{+0.21}_{-0.20}$	669^{+56}_{-59}	$2.7^{+2.3}_{-1.8}$	$2.3^{+2.0}_{-1.5}$	$1.67^{+1.11}_{-1.01}$	4.0×10^{-13}	Planet
228725791.02	$6.494351^{+0.002593}_{-0.002537}$	$2755.13589^{+0.01796}_{-0.01586}$	$18.6^{+3.7}_{-4.8}$	$0.0291^{+0.0028}_{-0.0030}$	$0.0516^{+0.0028}_{-0.0030}$	$1.21^{+0.23}_{-0.21}$	470^{+39}_{-39}	$2.8^{+2.6}_{-1.9}$	$1.7^{+1.6}_{-1.1}$	$2.05^{+1.49}_{-1.21}$	2.4×10^{-9}	Planet
228725972.01	$4.479015^{+0.001136}_{-0.001322}$	$2752.67214^{+0.01358}_{-0.01109}$	$13.3^{+2.7}_{-3.6}$	$0.0169^{+0.0017}_{-0.0015}$	$0.0534^{+0.0020}_{-0.0022}$	$2.28^{+0.86}_{-0.82}$	1246^{+208}_{-244}	$7.8^{+4.6}_{-4.4}$	$3.0^{+1.8}_{-1.7}$	$1.57^{+1.18}_{-0.96}$	1.7×10^{-5}	Planet
228725972.02	$10.094838^{+0.001211}_{-0.001147}$	$2755.41567^{+0.00430}_{-0.00410}$	$20.2^{+1.8}_{-4.4}$	$0.0265^{+0.0016}_{-0.0012}$	$0.0918^{+0.0035}_{-0.0038}$	$3.61^{+1.31}_{-1.27}$	951^{+159}_{-185}	$13.9^{+7.7}_{-6.3}$	$4.1^{+2.3}_{-1.8}$	$1.08^{+0.33}_{-0.56}$	5.5×10^{-5}	Planet
228729473.01	$16.772107^{+0.001849}_{-0.001909}$	$2752.76090^{+0.00388}_{-0.00347}$	$6.8^{+1.4}_{-1.1}$	$0.0448^{+0.0023}_{-0.0024}$	$0.1300^{+0.0045}_{-0.0049}$	$16.61^{+2.57}_{-2.50}$	1116^{+83}_{-87}	$98.1^{+68.0}_{-37.7}$	$23.8^{+16.6}_{-9.2}$	$0.01^{+0.01}_{-0.01}$	7.6×10^{-1}	False Positive
228732031.01	$0.369306^{+0.000009}_{-0.000009}$	$2749.93548^{+0.00107}_{-0.00106}$	$2.6^{+0.2}_{-0.4}$	$0.0207^{+0.0012}_{-0.0006}$	$0.0095^{+0.0001}_{-0.0001}$	$1.84^{+0.12}_{-0.09}$	2117^{+58}_{-58}	$6.0^{+2.4}_{-2.3}$	$5.8^{+2.3}_{-2.2}$	$1.67^{+0.41}_{-0.72}$	2.7×10^{-8}	Planet
228734900.01	$15.871971^{+0.003478}_{-0.003214}$	$2754.37552^{+0.00874}_{-0.00788}$	$17.6^{+1.9}_{-4.3}$	$0.0190^{+0.0013}_{-0.0009}$	$0.1287^{+0.0042}_{-0.0045}$	$3.93^{+0.70}_{-0.66}$	960^{+78}_{-83}	$15.5^{+5.2}_{-4.2}$	$3.6^{+1.3}_{-1.0}$	$0.29^{+0.10}_{-0.17}$	4.3×10^{-3}	Planet
228735255.01	$6.569181^{+0.000040}_{-0.000041}$	$2755.28513^{+0.00024}_{-0.00023}$	$15.1^{+0.1}_{-0.3}$	$0.1131^{+0.0007}_{-0.0005}$	$0.0686^{+0.0005}_{-0.0005}$	$12.22^{+0.14}_{-0.14}$	947^{+11}_{-11}	$67.2^{+32.7}_{-21.6}$	$22.9^{+11.2}_{-7.4}$	$1.08^{+0.03}_{-0.06}$	1.3×10^{-7}	Planet

Table 6 continued

Table 6 *(continued)*

EPIC	$P_{\rm orb}$ [days]	T_0 [BKJD]	a [$R_\star$]	R_P [$R_\star$]	a [AU]	R_P [$R_\oplus$]	$T_{\rm eq}$ [K]	M_P [$M_\oplus$]	$K_{\rm pred}$ [m s^{-1}]	$\rho_{\star,LC}$ [$\rho_\odot$]	FPP	Disposition
228736155.01	$3.271095^{+0.000469}_{-0.000492}$	$2751.02459^{+0.00588}_{-0.00561}$	$9.9^{+1.1}_{-2.1}$	$0.0154^{+0.0011}_{-0.0008}$	$0.0424^{+0.0020}_{-0.0022}$	$3.58^{+1.89}_{-1.87}$	1635^{+378}_{-462}	$14.1^{+10.6}_{-8.1}$	$6.3^{+4.9}_{-3.6}$	$1.22^{+0.44}_{-0.63}$	2.8×10^{-8}	Planet
228739306.01	$7.172473^{+0.001479}_{-0.001421}$	$2755.10461^{+0.00755}_{-0.00773}$	$16.1^{+1.8}_{-4.2}$	$0.0254^{+0.0019}_{-0.0014}$	$0.0702^{+0.0008}_{-0.0009}$	$2.39^{+0.25}_{-0.20}$	849^{+32}_{-32}	$8.4^{+2.6}_{-2.5}$	$3.0^{+0.9}_{-0.9}$	$1.09^{+0.41}_{-0.65}$	1.2×10^{-5}	Planet
228748383.01	$12.409126^{+0.003329}_{-0.002881}$	$2750.04553^{+0.01046}_{-0.01153}$	$14.6^{+1.7}_{-3.6}$	$0.0162^{+0.0014}_{-0.0012}$	$0.1062^{+0.0045}_{-0.0049}$	$1.94^{+0.77}_{-0.76}$	810^{+147}_{-175}	$6.3^{+4.1}_{-4.4}$	$1.7^{+1.1}_{-1.2}$	$0.27^{+0.10}_{-0.16}$	3.9×10^{-6}	Planet
228748826.01	$4.014551^{+0.000621}_{-0.000561}$	$2751.12162^{+0.00573}_{-0.00651}$	$12.0^{+1.6}_{-3.2}$	$0.0279^{+0.0026}_{-0.0017}$	$0.0462^{+0.0004}_{-0.0004}$	$2.33^{+0.23}_{-0.16}$	922^{+17}_{-17}	$8.1^{+2.6}_{-2.5}$	$3.7^{+1.2}_{-1.1}$	$1.45^{+0.67}_{-0.89}$	1.5×10^{-6}	Planet
228753871.01	$18.696536^{+0.004504}_{-0.004341}$	$2757.72887^{+0.01054}_{-0.01073}$	$64.5^{+11.2}_{-16.3}$	$0.0280^{+0.0029}_{-0.0024}$	$0.1335^{+0.0031}_{-0.0032}$	$2.64^{+0.77}_{-0.73}$	600^{+77}_{-86}	$9.4^{+4.5}_{-4.0}$	$2.4^{+1.2}_{-1.0}$	$10.28^{+6.38}_{-5.99}$	4.4×10^{-2}	Candidate
228758778.01	$9.300445^{+0.003309}_{-0.003600}$	$2756.07845^{+0.01529}_{-0.01171}$	$21.0^{+5.1}_{-7.1}$	$0.0435^{+0.0054}_{-0.0040}$	$0.0632^{+0.0031}_{-0.0034}$	$1.70^{+0.34}_{-0.28}$	393^{+29}_{-30}	$5.5^{+2.8}_{-2.5}$	$3.1^{+1.7}_{-1.4}$	$1.44^{+1.32}_{-1.03}$	7.4×10^{-6}	Planet
228758948.01	$12.202349^{+0.000719}_{-0.000704}$	$2753.82922^{+0.00230}_{-0.00240}$	$22.1^{+1.8}_{-4.8}$	$0.0370^{+0.0019}_{-0.0010}$	$0.1065^{+0.0007}_{-0.0007}$	$4.22^{+0.30}_{-0.26}$	819^{+23}_{-23}	$17.2^{+4.0}_{-3.5}$	$4.5^{+1.0}_{-0.9}$	$0.98^{+0.26}_{-0.50}$	1.4×10^{-4}	Candidate
228763938.01	$13.815242^{+0.004480}_{-0.004364}$	$2763.18980^{+0.01141}_{-0.01070}$	$25.4^{+3.4}_{-6.7}$	$0.0194^{+0.0019}_{-0.0013}$	$0.1050^{+0.0010}_{-0.0011}$	$1.63^{+0.17}_{-0.12}$	611^{+12}_{-13}	$5.2^{+2.4}_{-2.3}$	$1.6^{+0.7}_{-0.7}$	$1.15^{+0.52}_{-0.69}$	1.8×10^{-6}	Planet
228784812.01	$4.188649^{+0.001382}_{-0.001573}$	$2751.03254^{+0.01174}_{-0.01277}$	$18.8^{+11.6}_{-6.5}$	$0.0132^{+0.0020}_{-0.0019}$	$0.0479^{+0.0014}_{-0.0015}$	$1.19^{+0.23}_{-0.20}$	1009^{+53}_{-53}	$2.7^{+2.3}_{-1.8}$	$1.2^{+1.1}_{-0.8}$	$5.05^{+16.26}_{-3.63}$	1.8×10^{-1}	Candidate
228798746.01	$2.698273^{+0.000244}_{-0.000257}$	$2750.19426^{+0.00454}_{-0.00435}$	$11.8^{+1.4}_{-3.2}$	$0.0172^{+0.0018}_{-0.0009}$	$0.0338^{+0.0008}_{-0.0009}$	$1.22^{+0.15}_{-0.12}$	880^{+46}_{-45}	$3.0^{+2.0}_{-1.7}$	$1.7^{+1.2}_{-1.0}$	$3.01^{+1.24}_{-1.85}$	2.4×10^{-3}	Planet
228801451.01	$0.584259^{+0.000017}_{-0.000017}$	$2750.46901^{+0.00123}_{-0.00120}$	$3.4^{+0.2}_{-0.6}$	$0.0133^{+0.0008}_{-0.0004}$	$0.0131^{+0.0001}_{-0.0001}$	$1.16^{+0.07}_{-0.04}$	1844^{+19}_{-19}	$2.9^{+1.4}_{-1.6}$	$2.3^{+1.1}_{-1.3}$	$1.51^{+0.36}_{-0.71}$	2.2×10^{-9}	Planet
228801451.02	$8.327268^{+0.000423}_{-0.000432}$	$2753.34307^{+0.00196}_{-0.00191}$	$24.5^{+2.4}_{-7.1}$	$0.0237^{+0.0022}_{-0.0007}$	$0.0771^{+0.0003}_{-0.0003}$	$2.07^{+0.19}_{-0.07}$	760^{+8}_{-8}	$7.1^{+2.4}_{-2.3}$	$2.4^{+0.8}_{-0.8}$	$2.84^{+0.92}_{-1.82}$	7.9×10^{-6}	Planet
228804845.01	$2.860403^{+0.000622}_{-0.000598}$	$2749.59183^{+0.00918}_{-0.00922}$	$7.3^{+1.4}_{-1.7}$	$0.0129^{+0.0011}_{-0.0010}$	$0.0405^{+0.0002}_{-0.0002}$	$1.55^{+0.24}_{-0.22}$	1365^{+79}_{-84}	$4.8^{+2.5}_{-2.3}$	$2.0^{+1.0}_{-1.0}$	$0.63^{+0.43}_{-0.35}$	7.9×10^{-5}	Planet
228809391.01	$19.578663^{+0.005274}_{-0.004929}$	$2763.80364^{+0.00748}_{-0.00809}$	$53.4^{+5.1}_{-10.1}$	$0.0268^{+0.0017}_{-0.0016}$	$0.1396^{+0.0016}_{-0.0015}$	$2.62^{+0.22}_{-0.20}$	624^{+19}_{-20}	$9.3^{+2.6}_{-2.5}$	$2.3^{+0.6}_{-0.6}$	$5.32^{+1.68}_{-2.48}$	1.0×10^{-2}	Candidate
228809550.01	$4.001558^{+0.000107}_{-0.000112}$	$2750.99951^{+0.00132}_{-0.00127}$	$13.0^{+2.2}_{-1.6}$	$0.1123^{+0.0047}_{-0.0047}$	$0.0457^{+0.0015}_{-0.0015}$	$9.34^{+1.01}_{-0.99}$	940^{+56}_{-56}	$47.1^{+20.9}_{-13.7}$	$22.1^{+9.9}_{-6.6}$	$1.82^{+1.09}_{-0.61}$	8.9×10^{-5}	Planet
228834632.01	$11.741950^{+0.007845}_{-0.008238}$	$2758.58188^{+0.02924}_{-0.03041}$	$25.6^{+5.8}_{-7.2}$	$0.0277^{+0.0034}_{-0.0033}$	$0.0831^{+0.0021}_{-0.0022}$	$1.47^{+0.24}_{-0.22}$	440^{+23}_{-23}	$4.4^{+2.5}_{-2.3}$	$1.8^{+1.1}_{-1.0}$	$1.64^{+1.39}_{-1.02}$	1.7×10^{-2}	Candidate
228836835.01	$0.728121^{+0.000135}_{-0.000147}$	$2750.26218^{+0.00805}_{-0.00766}$	$7.5^{+0.7}_{-0.9}$	$0.0269^{+0.0042}_{-0.0043}$	$0.0111^{+0.0009}_{-0.0010}$	$0.93^{+0.26}_{-0.24}$	902^{+104}_{-107}	$0.9^{+2.1}_{-0.8}$	$1.4^{+3.2}_{-1.1}$	$10.61^{+3.26}_{-3.29}$	7.4×10^{-2}	Candidate
228846243.01	$25.582218^{+0.023557}_{-0.019652}$	$2756.86945^{+0.03209}_{-0.03512}$	$22.3^{+5.7}_{-6.4}$	$0.0401^{+0.0048}_{-0.0038}$	$0.1731^{+0.0046}_{-0.0047}$	$8.03^{+1.54}_{-1.33}$	792^{+59}_{-59}	$38.6^{+19.2}_{-11.9}$	$8.1^{+4.0}_{-2.6}$	$0.23^{+0.22}_{-0.14}$	1.2×10^{-1}	Candidate
228849382.01	$4.096313^{+0.000803}_{-0.000784}$	$2749.97657^{+0.00976}_{-0.01029}$	$15.8^{+0.7}_{-0.8}$	$0.0224^{+0.0038}_{-0.0034}$	$0.0437^{+0.0011}_{-0.0011}$	$1.45^{+0.29}_{-0.25}$	711^{+39}_{-38}	$4.3^{+2.7}_{-2.4}$	$2.3^{+1.4}_{-1.3}$	$3.14^{+0.44}_{-0.44}$	3.1×10^{-4}	Planet
228849382.02	$12.118335^{+0.003363}_{-0.003474}$	$2757.61339^{+0.01149}_{-0.01133}$	$30.7^{+5.2}_{-8.1}$	$0.0300^{+0.0033}_{-0.0026}$	$0.0901^{+0.0021}_{-0.0023}$	$1.95^{+0.29}_{-0.24}$	495^{+27}_{-26}	$6.5^{+2.6}_{-2.5}$	$2.4^{+1.0}_{-0.9}$	$2.65^{+1.58}_{-1.60}$	2.5×10^{-7}	Planet
228888935.01	$5.690487^{+0.000272}_{-0.000269}$	$2751.67076^{+0.00208}_{-0.00202}$	$8.0^{+1.9}_{-0.7}$	$0.0886^{+0.0028}_{-0.0051}$	$0.0589^{+0.0021}_{-0.0022}$	$7.76^{+1.29}_{-1.26}$	893^{+73}_{-77}	$36.6^{+16.5}_{-10.8}$	$14.7^{+6.8}_{-4.4}$	$0.21^{+0.19}_{-0.05}$	3.5×10^{-4}	Planet
228894622.01	$1.964155^{+0.000042}_{-0.000042}$	$2750.30160^{+0.00089}_{-0.00089}$	$9.3^{+0.7}_{-1.9}$	$0.0382^{+0.0028}_{-0.0010}$	$0.0271^{+0.0004}_{-0.0004}$	$2.77^{+0.21}_{-0.14}$	1004^{+27}_{-27}	$10.1^{+2.6}_{-2.5}$	$6.6^{+1.7}_{-1.6}$	$2.78^{+0.66}_{-1.36}$	1.3×10^{-8}	Planet
228934525.01	$3.676261^{+0.000307}_{-0.000318}$	$2752.05333^{+0.00383}_{-0.00364}$	$14.6^{+2.0}_{-3.7}$	$0.0289^{+0.0026}_{-0.0016}$	$0.0380^{+0.0007}_{-0.0007}$	$1.67^{+0.18}_{-0.13}$	696^{+31}_{-30}	$5.4^{+2.4}_{-2.3}$	$3.3^{+1.5}_{-1.4}$	$3.12^{+1.42}_{-1.82}$	9.2×10^{-11}	Planet
228934525.02	$7.954847^{+0.000818}_{-0.000820}$	$2751.33759^{+0.00437}_{-0.00424}$	$25.2^{+2.8}_{-5.5}$	$0.0302^{+0.0023}_{-0.0018}$	$0.0636^{+0.0011}_{-0.0012}$	$1.74^{+0.17}_{-0.14}$	538^{+23}_{-23}	$5.6^{+2.4}_{-2.3}$	$2.7^{+1.2}_{-1.1}$	$3.41^{+1.26}_{-1.78}$	5.8×10^{-10}	Planet
228964773.01	$37.203998^{+0.013222}_{-0.015691}$	$2776.76384^{+0.01254}_{-0.01093}$	$55.2^{+9.8}_{-14.2}$	$0.0546^{+0.0056}_{-0.0045}$	$0.2091^{+0.0021}_{-0.0021}$	$5.11^{+0.67}_{-0.54}$	496^{+17}_{-17}	$21.9^{+6.9}_{-5.1}$	$4.5^{+1.5}_{-1.1}$	$1.63^{+1.03}_{-0.96}$	7.7×10^{-3}	Candidate
228968232.01	$5.520042^{+0.002314}_{-0.002748}$	$2753.52550^{+0.01926}_{-0.01970}$	$7.7^{+1.2}_{-1.9}$	$0.0306^{+0.0028}_{-0.0022}$	$0.0561^{+0.0019}_{-0.0020}$	$2.48^{+1.00}_{-0.98}$	853^{+154}_{-186}	$8.7^{+5.3}_{-5.0}$	$3.7^{+2.3}_{-2.1}$	$0.20^{+0.11}_{-0.11}$	1.7×10^{-7}	Planet
228974324.01	$1.605888^{+0.000131}_{-0.000131}$	$2750.28750^{+0.00350}_{-0.00364}$	$8.2^{+1.1}_{-1.9}$	$0.0154^{+0.0012}_{-0.0009}$	$0.0178^{+0.0002}_{-0.0003}$	$0.47^{+0.04}_{-0.03}$	634^{+15}_{-14}	$0.1^{+0.1}_{-0.1}$	$0.1^{+0.1}_{-0.1}$	$2.82^{+1.26}_{-1.57}$	$< 10^{-13}$	Planet
228974907.01	$20.851664^{+0.024597}_{-0.032266}$	$2759.60767^{+0.05965}_{-0.04396}$	$34.6^{+7.3}_{-10.8}$	$0.0103^{+0.0010}_{-0.0010}$	$0.1839^{+0.0038}_{-0.0040}$	$3.18^{+0.57}_{-0.56}$	1227^{+98}_{-106}	$11.9^{+4.0}_{-3.6}$	$1.8^{+0.6}_{-0.5}$	$1.28^{+1.00}_{-0.86}$	1.1×10^{-2}	Candidate
229004835.01	$16.136768^{+0.001847}_{-0.001899}$	$2764.62906^{+0.00384}_{-0.00391}$	$54.9^{+4.8}_{-10.0}$	$0.0184^{+0.0008}_{-0.0007}$	$0.1219^{+0.0007}_{-0.0007}$	$1.96^{+0.17}_{-0.17}$	726^{+27}_{-29}	$6.4^{+2.4}_{-2.4}$	$1.7^{+0.6}_{-0.6}$	$8.51^{+2.42}_{-3.86}$	4.5×10^{-2}	Candidate
229017395.01	$19.092088^{+0.006334}_{-0.006618}$	$2753.29270^{+0.01561}_{-0.01358}$	$21.5^{+2.1}_{-4.8}$	$0.0205^{+0.0015}_{-0.0014}$	$0.1407^{+0.0050}_{-0.0053}$	$2.83^{+0.60}_{-0.57}$	809^{+78}_{-84}	$10.3^{+3.9}_{-3.5}$	$2.4^{+1.0}_{-0.9}$	$0.37^{+0.12}_{-0.20}$	6.8×10^{-6}	Planet
229103251.01	$11.671990^{+0.004388}_{-0.003825}$	$2756.70532^{+0.01314}_{-0.01304}$	$28.4^{+7.8}_{-8.9}$	$0.0280^{+0.0031}_{-0.0023}$	$0.0976^{+0.0033}_{-0.0034}$	$2.94^{+0.73}_{-0.66}$	793^{+82}_{-93}	$10.9^{+4.3}_{-3.7}$	$3.3^{+1.4}_{-1.1}$	$2.26^{+2.40}_{-1.53}$	6.0×10^{-2}	Candidate
229131722.01	$15.480428^{+0.003391}_{-0.004039}$	$2752.70933^{+0.01036}_{-0.01025}$	$30.1^{+4.5}_{-7.2}$	$0.0189^{+0.0015}_{-0.0013}$	$0.1259^{+0.0017}_{-0.0018}$	$2.26^{+0.26}_{-0.24}$	780^{+35}_{-35}	$7.8^{+2.6}_{-2.5}$	$1.9^{+0.6}_{-0.6}$	$1.53^{+0.78}_{-0.86}$	2.3×10^{-3}	Planet
229133720.01	$4.036929^{+0.000129}_{-0.000130}$	$2750.96334^{+0.00125}_{-0.00131}$	$13.4^{+0.9}_{-2.4}$	$0.0285^{+0.0016}_{-0.0007}$	$0.0481^{+0.0024}_{-0.0027}$	$7.37^{+4.33}_{-4.27}$	1564^{+391}_{-476}	$34.4^{+35.0}_{-20.5}$	$14.7^{+15.3}_{-8.8}$	$1.97^{+0.43}_{-0.89}$	4.7×10^{-12}	Candidate

Table 7. Stellar parameters used in this work, where 'Provenance' indicates the source of the parameters.

EPIC	$T_{\rm eff}$ [K]	log g [cgs]	[Fe/H] [dex]	Mass [$M_\odot$]	Radius [$R_\odot$]	$v\sin i$ [km/s]	Provenance
201092629	5100 ± 71	4.38 ± 0.16	-0.50 ± 0.04	$0.71^{+0.02}_{-0.02}$	$0.67^{+0.02}_{-0.02}$	2.08 ± 0.29	This work
201102594	3732^{+112}_{-90}	4.96 ± 0.05	$-0.11^{+0.24}_{-0.16}$	0.34 ± 0.06	$0.32^{+0.05}_{-0.05}$	—	H16
201110617	4480 ± 66	4.56 ± 0.19	-0.44 ± 0.08	$0.62^{+0.02}_{-0.02}$	$0.60^{+0.02}_{-0.02}$	1.80 ± 0.30	This work
201111557	4620 ± 166	$4.65^{+0.04}_{-0.03}$	$-0.03^{+0.10}_{-0.12}$	$0.73^{+0.05}_{-0.04}$	$0.67^{+0.04}_{-0.04}$	—	H16
201127519	4900 ± 63	4.50 ± 0.18	0.01 ± 0.06	$0.80^{+0.02}_{-0.03}$	$0.75^{+0.02}_{-0.02}$	1.85 ± 0.22	This work
201128338	4280 ± 136	4.25 ± 0.42	-0.74 ± 0.10	$0.55^{+0.03}_{-0.03}$	$0.53^{+0.03}_{-0.03}$	3.70 ± 0.30	This work
201132684	5549 ± 89	$4.51^{+0.04}_{-0.04}$	$-0.15^{+0.18}_{-0.21}$	$0.90^{+0.07}_{-0.09}$	$0.88^{+0.06}_{-0.07}$	—	H16
201164625	6160 ± 93	3.50 ± 0.35	0.18 ± 0.03	$1.29^{+0.22}_{-0.11}$	$1.64^{+0.65}_{-0.42}$	11.50 ± 0.46	This work
201166680	6714^{+159}_{-132}	$4.24^{+0.06}_{-0.08}$	$-0.14^{+0.12}_{-0.36}$	$1.29^{+0.09}_{-0.18}$	$1.39^{+0.18}_{-0.13}$	—	H16
201180665	5922^{+143}_{-179}	$4.33^{+0.11}_{-0.31}$	$-0.40^{+0.30}_{-0.36}$	$0.93^{+0.10}_{-0.08}$	$1.07^{+0.46}_{-0.18}$	—	H16
201211526	5660 ± 40	4.44 ± 0.12	-0.30 ± 0.03	$0.87^{+0.02}_{-0.02}$	$0.85^{+0.09}_{-0.04}$	3.69 ± 0.24	This work
201225286	5538^{+111}_{-89}	4.55 ± 0.03	$-0.53^{+0.25}_{-0.30}$	$0.79^{+0.07}_{-0.06}$	$0.78^{+0.05}_{-0.06}$	—	H16
201274010	5668^{+113}_{-91}	$4.47^{+0.04}_{-0.31}$	-0.24 ± 0.25	0.93 ± 0.08	$0.93^{+0.34}_{-0.10}$	—	H16
201352100	5240 ± 68	4.81 ± 0.12	-0.02 ± 0.04	$0.87^{+0.02}_{-0.02}$	$0.80^{+0.02}_{-0.02}$	2.15 ± 0.30	This work
201357643	5660 ± 93	3.94 ± 0.16	-0.46 ± 0.02	$0.87^{+0.08}_{-0.04}$	$1.53^{+0.32}_{-0.30}$	4.62 ± 0.24	This work
201386739	5600 ± 32	4.38 ± 0.07	-0.20 ± 0.03	$0.87^{+0.02}_{-0.02}$	$0.94^{+0.07}_{-0.07}$	2.90 ± 0.30	This work
201390048	4717 ± 94	$4.64^{+0.04}_{-0.03}$	$-0.09^{+0.12}_{-0.27}$	$0.75^{+0.04}_{-0.08}$	$0.68^{+0.04}_{-0.06}$	—	H16
201390927	4166^{+83}_{-66}	$4.76^{+0.04}_{-0.03}$	$-0.04^{+0.15}_{-0.12}$	$0.58^{+0.04}_{-0.03}$	$0.53^{+0.03}_{-0.03}$	—	H16
201392505	5100 ± 63	4.75 ± 0.10	-0.20 ± 0.07	$0.79^{+0.03}_{-0.03}$	$0.74^{+0.02}_{-0.02}$	2.46 ± 0.29	This work
201437844	6254^{+55}_{-51}	$4.23^{+0.04}_{-0.03}$	$-0.28^{+0.08}_{-0.07}$	1.03 ± 0.03	$1.28^{+0.05}_{-0.06}$	12.90 ± 0.40	Rodriguez et al. 2017
201595106	5820 ± 20	4.62 ± 0.12	-0.01 ± 0.03	$1.02^{+0.01}_{-0.01}$	$0.96^{+0.04}_{-0.02}$	3.62 ± 0.18	This work
201598502	3830^{+76}_{-60}	$4.88^{+0.04}_{-0.06}$	$0.05^{+0.12}_{-0.08}$	$0.45^{+0.05}_{-0.06}$	$0.40^{+0.05}_{-0.04}$	—	H16
201615463	5874^{+141}_{-176}	$3.94^{+0.12}_{-0.10}$	$-0.15^{+0.12}_{-0.15}$	$1.14^{+0.13}_{-0.11}$	$1.83^{+0.31}_{-0.26}$	—	H16
228707509	5312 ± 108	$4.55^{+0.06}_{-0.98}$	$-0.48^{+0.35}_{-0.56}$	$0.81^{+0.08}_{-0.10}$	$0.79^{+1.72}_{-0.11}$	—	H16
228720681	5680 ± 86	4.25 ± 0.14	-0.28 ± 0.04	$0.87^{+0.03}_{-0.03}$	$0.95^{+0.15}_{-0.10}$	12.00 ± 0.60	This work
228721452	6013 ± 122	4.12 ± 0.23	$0.05^{+0.12}_{-0.15}$	$1.19^{+0.21}_{-0.13}$	$1.51^{+0.70}_{-0.41}$	—	H16
228724899	5500 ± 55	4.50 ± 0.10	0.17 ± 0.04	$0.96^{+0.02}_{-0.03}$	$0.90^{+0.06}_{-0.03}$	2.90 ± 0.30	This work
228725791	3891 ± 92	$4.89^{+0.08}_{-0.04}$	$-0.11^{+0.12}_{-0.15}$	$0.44^{+0.07}_{-0.08}$	$0.39^{+0.05}_{-0.06}$	—	H16
228725972	5846^{+137}_{-172}	$4.21^{+0.24}_{-0.32}$	$-0.15^{+0.20}_{-0.36}$	$1.01^{+0.11}_{-0.13}$	$1.24^{+0.61}_{-0.32}$	—	H16
228729473	4940 ± 51	3.38 ± 0.12	-0.05 ± 0.02	$1.04^{+0.14}_{-0.09}$	$3.40^{+0.57}_{-0.43}$	3.46 ± 0.27	This work
228732031	5200 ± 100	4.62 ± 0.10	0.00 ± 0.08	0.84 ± 0.03	0.81 ± 0.03	4.40 ± 1.00	Dai et al. 2017
228734900	5691^{+138}_{-92}	$3.90^{+0.14}_{-0.10}$	-0.04 ± 0.24	1.13 ± 0.12	$1.88^{+0.30}_{-0.30}$	—	H16
228735255	5654 ± 55	4.45 ± 0.01	0.12 ± 0.04	1.00 ± 0.02	0.99 ± 0.01	3.80 ± 0.20	Giles et al. 2017
228736155	5205 ± 124	$3.81^{+0.73}_{-0.34}$	$-0.10^{+0.20}_{-0.40}$	$0.95^{+0.25}_{-0.08}$	$2.11^{+0.91}_{-1.35}$	—	H16
228739306	5500 ± 100	4.44 ± 0.16	-0.11 ± 0.04	$0.90^{+0.03}_{-0.03}$	$0.86^{+0.08}_{-0.04}$	2.60 ± 0.20	This work
228748383	5714^{+114}_{-160}	$4.36^{+0.12}_{-0.54}$	$-0.01^{+0.20}_{-0.28}$	$1.04^{+0.17}_{-0.11}$	$1.09^{+1.07}_{-0.17}$	—	H16
228748826	5140 ± 51	4.62 ± 0.16	-0.11 ± 0.04	$0.82^{+0.02}_{-0.03}$	$0.77^{+0.03}_{-0.02}$	2.20 ± 0.30	This work
228753871	5350^{+108}_{-152}	$4.51^{+0.04}_{-0.69}$	$-0.05^{+0.12}_{-0.18}$	$0.91^{+0.10}_{-0.04}$	$0.86^{+1.22}_{-0.04}$	—	H16
228758778	3745 ± 75	$4.91^{+0.08}_{-0.04}$	0.02 ± 0.12	$0.39^{+0.04}_{-0.08}$	$0.36^{+0.04}_{-0.06}$	—	H16
228758948	5940 ± 60	4.69 ± 0.19	0.11 ± 0.03	$1.08^{+0.02}_{-0.02}$	$1.04^{+0.08}_{-0.04}$	4.40 ± 0.20	This work
228763938	5120 ± 49	4.50 ± 0.10	-0.11 ± 0.04	$0.81^{+0.02}_{-0.02}$	$0.77^{+0.04}_{-0.02}$	2.20 ± 0.20	This work
228784812	5506^{+100}_{-166}	$4.52^{+0.04}_{-0.05}$	$-0.28^{+0.20}_{-0.24}$	$0.84^{+0.09}_{-0.07}$	$0.83^{+0.09}_{-0.06}$	—	H16
228798746	4584 ± 140	$4.66^{+0.04}_{-0.03}$	$-0.10^{+0.12}_{-0.15}$	$0.71^{+0.05}_{-0.06}$	$0.64^{+0.05}_{-0.05}$	—	H16
228801451	5360 ± 40	4.81 ± 0.06	-0.08 ± 0.02	$0.88^{+0.01}_{-0.01}$	$0.80^{+0.01}_{-0.01}$	2.46 ± 0.22	This work
228804845	5940 ± 24	4.25 ± 0.18	0.10 ± 0.04	$1.09^{+0.02}_{-0.02}$	$1.10^{+0.22}_{-0.08}$	5.20 ± 0.20	This work
228809391	5580 ± 97	4.50 ± 0.10	-0.01 ± 0.03	$0.95^{+0.03}_{-0.03}$	$0.90^{+0.06}_{-0.04}$	3.20 ± 0.20	This work
228809550	5224^{+128}_{-160}	$4.58^{+0.04}_{-0.05}$	$-0.27^{+0.25}_{-0.40}$	$0.80^{+0.07}_{-0.09}$	$0.76^{+0.07}_{-0.08}$	—	H16
228834632	4109^{+97}_{-81}	$4.80^{+0.03}_{-0.04}$	$-0.03^{+0.12}_{-0.18}$	$0.56^{+0.05}_{-0.04}$	$0.49^{+0.05}_{-0.04}$	—	H16
228836835	3782 ± 152	$4.96^{+0.06}_{-0.07}$	-0.18 ± 0.25	$0.34^{+0.08}_{-0.10}$	$0.32^{+0.07}_{-0.07}$	—	H16
228846243	5517 ± 130	$3.94^{+0.13}_{-0.09}$	$-0.03^{+0.12}_{-0.15}$	$1.06^{+0.10}_{-0.08}$	$1.84^{+0.22}_{-0.30}$	—	H16
228849382	4368^{+134}_{-107}	4.70 ± 0.04	-0.02 ± 0.15	0.66 ± 0.05	$0.59^{+0.05}_{-0.06}$	—	H16

Table 7 continued

Table 7 *(continued)*

EPIC	$T_{\rm eff}$ [K]	log g [cgs]	[Fe/H] [dex]	Mass [$M_\odot$]	Radius [$R_\odot$]	$v\sin i$ [km/s]	Provenance
228888935	5451 ± 130	$4.53^{+0.05}_{-0.13}$	$-0.37^{+0.30}_{-0.48}$	$0.84^{+0.09}_{-0.10}$	$0.81^{+0.20}_{-0.08}$	—	H16
228894622	4620 ± 80	4.56 ± 0.12	-0.27 ± 0.10	$0.69^{+0.03}_{-0.03}$	$0.66^{+0.03}_{-0.02}$	2.46 ± 0.27	This work
228934525	4240 ± 136	4.00 ± 0.37	-0.72 ± 0.09	$0.54^{+0.03}_{-0.03}$	$0.53^{+0.03}_{-0.03}$	2.90 ± 0.40	This work
228964773	5560 ± 68	4.44 ± 0.12	-0.19 ± 0.03	$0.88^{+0.03}_{-0.03}$	$0.86^{+0.08}_{-0.04}$	3.40 ± 0.20	This work
228968232	5327 ± 130	$4.58^{+0.03}_{-0.93}$	-0.61 ± 0.25	$0.77^{+0.10}_{-0.06}$	$0.74^{+1.58}_{-0.05}$	—	H16
228974324	3619^{+36}_{-72}	5.01 ± 0.02	$-0.01^{+0.08}_{-0.05}$	$0.29^{+0.01}_{-0.03}$	$0.28^{+0.01}_{-0.01}$	—	H16
228974907	7113 ± 290	$3.80^{+0.10}_{-0.12}$	$0.07^{+0.12}_{-0.10}$	1.91 ± 0.12	$2.81^{+0.44}_{-0.38}$	—	H16
229004835	5820 ± 37	4.38 ± 0.07	-0.22 ± 0.01	$0.93^{+0.02}_{-0.01}$	$0.97^{+0.08}_{-0.07}$	3.77 ± 0.12	This work
229017395	6103 ± 97	$4.20^{+0.17}_{-0.14}$	$-0.29^{+0.20}_{-0.32}$	$1.02^{+0.10}_{-0.12}$	$1.27^{+0.25}_{-0.25}$	—	H16
229103251	5719^{+232}_{-185}	$4.44^{+0.07}_{-0.20}$	$-0.30^{+0.30}_{-0.48}$	0.91 ± 0.09	$0.96^{+0.28}_{-0.14}$	—	H16
229131722	6000 ± 126	4.44 ± 0.12	0.17 ± 0.04	$1.11^{+0.05}_{-0.05}$	$1.09^{+0.10}_{-0.07}$	5.23 ± 0.20	This work
229133720	5000^{+99}_{-79}	$3.64^{+0.95}_{-0.40}$	$-0.23^{+0.25}_{-0.30}$	$0.92^{+0.17}_{-0.12}$	$2.33^{+1.15}_{-1.63}$	—	H16

Table 8. Individual false positive scenario likelihoods computed by `vespa`. Note: a – likelihood that the signal is due to a background eclipsing binary, at the measured period or twice that; b – likelihood that the signal is due to an eclipsing binary, at the measured period or twice that; c – likelihood that the signal is due to a hierarchical star system with an eclipsing component, at the measured period or twice that; d – likelihood that the signal is due to a planet.

EPIC	L_beb[a]	L_beb_Px2[a]	L_eb[b]	L_eb_Px2[b]	L_heb[c]	L_heb_Px2[c]	L_pl[d]	FPP
201092629.01	0	0	2.1×10^{-15}	3.1×10^{-9}	4.0×10^{-21}	2.3×10^{-12}	8.6×10^{-3}	3.6×10^{-7}
201102594.01	0	0	2.5×10^{-22}	1.1×10^{-11}	7.3×10^{-22}	2.7×10^{-13}	2.9×10^{-2}	4.0×10^{-10}
201110617.01	0	0	2.0×10^{-29}	4.2×10^{-11}	1.2×10^{-19}	2.3×10^{-11}	1.7×10^{-1}	3.9×10^{-10}
201111557.01	0	0	2.3×10^{-10}	2.7×10^{-7}	7.4×10^{-11}	1.0×10^{-7}	4.5×10^{-3}	8.3×10^{-5}
201127519.01	3.3×10^{-14}	0	4.8×10^{-4}	4.5×10^{-6}	1.0×10^{-5}	2.1×10^{-8}	2.5×10^{-2}	2.0×10^{-2}
201128338.01	0	0	6.4×10^{-6}	5.8×10^{-6}	2.4×10^{-7}	4.6×10^{-7}	1.2×10^{-3}	1.0×10^{-2}
201132684.01	0	0	6.6×10^{-28}	8.3×10^{-11}	1.4×10^{-29}	2.2×10^{-13}	1.9×10^{-3}	4.5×10^{-8}
201132684.02	0	0	2.5×10^{-14}	4.3×10^{-9}	1.2×10^{-22}	1.5×10^{-14}	1.8×10^{-2}	2.3×10^{-7}
201164625.01	0	0	3.1×10^{-6}	3.4×10^{-6}	1.4×10^{-7}	7.1×10^{-8}	7.4×10^{-3}	9.0×10^{-4}
201166680.01	1.4×10^{-5}	1.7×10^{-6}	4.2×10^{-7}	1.7×10^{-9}	4.3×10^{-20}	3.1×10^{-15}	9.6×10^{-3}	1.7×10^{-3}
201166680.02	5.4×10^{-6}	1.9×10^{-6}	1.9×10^{-7}	4.8×10^{-8}	5.4×10^{-16}	4.2×10^{-12}	2.3×10^{-3}	3.3×10^{-3}
201180665.01	0	0	4.4×10^{-4}	2.8×10^{-7}	5.5×10^{-6}	5.2×10^{-10}	1.6×10^{-3}	2.1×10^{-1}
201211526.01	0	0	7.4×10^{-6}	5.1×10^{-6}	1.5×10^{-16}	3.4×10^{-11}	5.9×10^{-3}	2.1×10^{-3}
201225286.01	0	0	2.8×10^{-9}	4.1×10^{-7}	1.8×10^{-10}	3.5×10^{-10}	2.1×10^{-2}	1.9×10^{-5}
201274010.01	3.4×10^{-4}	6.0×10^{-4}	3.4×10^{-5}	4.9×10^{-5}	1.0×10^{-8}	1.2×10^{-7}	5.5×10^{-3}	1.6×10^{-1}
201352100.01	0	8.7×10^{-10}	8.9×10^{-7}	3.8×10^{-8}	8.1×10^{-9}	1.1×10^{-9}	2.7×10^{-2}	3.5×10^{-5}
201357643.01	3.1×10^{-12}	0	0	0	6.3×10^{-311}	1.9×10^{-100}	2.4×10^{-2}	1.3×10^{-10}
201386739.01	0	0	1.0×10^{-14}	5.7×10^{-7}	3.0×10^{-19}	4.6×10^{-10}	5.8×10^{-3}	9.8×10^{-5}
201390048.01	5.1×10^{-5}	5.2×10^{-6}	1.2×10^{-19}	2.4×10^{-11}	2.6×10^{-19}	5.1×10^{-11}	2.4×10^{-2}	2.3×10^{-3}
201390927.01	0	0	9.9×10^{-18}	9.4×10^{-12}	3.1×10^{-17}	4.2×10^{-11}	3.0×10^{-3}	1.7×10^{-8}
201392505.01	0	0	6.1×10^{-23}	1.5×10^{-12}	2.4×10^{-44}	3.6×10^{-16}	1.5×10^{-4}	9.7×10^{-9}
201437844.01	0	0	2.4×10^{-6}	7.0×10^{-6}	3.8×10^{-8}	6.0×10^{-8}	5.7×10^{-3}	1.7×10^{-3}
201437844.02	0	0	6.7×10^{-8}	4.2×10^{-7}	7.0×10^{-10}	1.6×10^{-9}	2.9×10^{-3}	1.7×10^{-4}
201595106.01	0	0	1.8×10^{-5}	2.2×10^{-4}	1.7×10^{-6}	1.3×10^{-5}	2.0×10^{-1}	1.3×10^{-3}
201598502.01	0	0	1.6×10^{-8}	8.0×10^{-7}	1.8×10^{-9}	6.4×10^{-8}	1.0×10^{-2}	8.6×10^{-5}
201615463.01	3.3×10^{-6}	4.3×10^{-6}	1.3×10^{-6}	2.0×10^{-7}	5.8×10^{-8}	6.5×10^{-9}	6.2×10^{-3}	1.5×10^{-3}
228707509.01	0	0	4.8×10^{-10}	3.2×10^{-7}	6.5×10^{-19}	1.5×10^{-13}	1.4×10^{-2}	2.3×10^{-5}
228720681.01	0	0	8.6×10^{-4}	1.7×10^{-5}	3.2×10^{-6}	1.7×10^{-7}	1.8×10^{-2}	4.8×10^{-2}
228721452.01	0	0	3.9×10^{-6}	3.4×10^{-4}	6.4×10^{-7}	4.2×10^{-5}	7.0×10^{-2}	5.5×10^{-3}
228721452.02	0	0	2.7×10^{-5}	5.8×10^{-6}	8.8×10^{-7}	1.2×10^{-7}	1.2×10^{-2}	2.9×10^{-3}
228724899.01	0	0	1.8×10^{-3}	3.5×10^{-4}	4.1×10^{-5}	8.6×10^{-6}	1.4×10^{-2}	1.4×10^{-1}
228725791.01	0	0	9.4×10^{-24}	1.1×10^{-13}	3.1×10^{-22}	6.4×10^{-14}	1.8×10^{-2}	1.0×10^{-11}
228725791.02	0	0	7.0×10^{-17}	1.8×10^{-10}	9.2×10^{-15}	1.5×10^{-10}	5.5×10^{-3}	6.0×10^{-8}
228725972.01	0	0	1.2×10^{-6}	4.7×10^{-6}	4.4×10^{-10}	1.1×10^{-7}	1.4×10^{-2}	4.3×10^{-4}
228725972.02	0	0	4.5×10^{-6}	7.9×10^{-6}	1.2×10^{-9}	1.5×10^{-8}	9.0×10^{-3}	1.4×10^{-3}
228729473.01	0	0	4.9×10^{-3}	4.8×10^{-6}	0	1.5×10^{-49}	1.5×10^{-3}	7.6×10^{-1}

Table 8 continued

Table 8 *(continued)*

EPIC	L_beb[a]	L_beb_Px2[a]	L_eb[b]	L_eb_Px2[b]	L_heb[c]	L_heb_Px2[c]	L_pl[d]	FPP
228732031.01	0	0	2.8×10^{-50}	1.9×10^{-10}	4.3×10^{-14}	2.0×10^{-7}	7.2×10^{0}	2.7×10^{-8}
228734900.01	9.9×10^{-6}	3.2×10^{-6}	7.3×10^{-8}	4.2×10^{-7}	1.1×10^{-16}	1.0×10^{-8}	3.2×10^{-3}	4.3×10^{-3}
228735255.01	0	0	4.0×10^{-11}	5.3×10^{-9}	7.3×10^{-17}	6.5×10^{-10}	4.5×10^{-2}	1.3×10^{-7}
228736155.01	0	0	1.0×10^{-10}	1.1×10^{-9}	6.9×10^{-29}	1.0×10^{-13}	4.3×10^{-2}	2.8×10^{-8}
228739306.01	0	0	6.0×10^{-9}	4.6×10^{-7}	5.3×10^{-12}	9.5×10^{-10}	4.0×10^{-2}	1.2×10^{-5}
228748383.01	0	0	1.7×10^{-9}	6.8×10^{-10}	1.2×10^{-17}	2.0×10^{-10}	6.6×10^{-4}	3.9×10^{-6}
228748826.01	0	0	1.2×10^{-13}	1.4×10^{-7}	2.4×10^{-12}	1.0×10^{-8}	1.0×10^{-1}	1.5×10^{-6}
228753871.01	2.3×10^{-5}	2.3×10^{-5}	2.3×10^{-5}	4.4×10^{-6}	1.7×10^{-7}	1.7×10^{-7}	1.6×10^{-3}	4.4×10^{-2}
228758778.01	0	1.7×10^{-8}	5.6×10^{-17}	2.8×10^{-9}	4.8×10^{-20}	6.1×10^{-11}	2.7×10^{-3}	7.4×10^{-6}
228758948.01	0	0	1.6×10^{-6}	1.9×10^{-6}	2.0×10^{-9}	8.5×10^{-8}	2.6×10^{-2}	1.4×10^{-4}
228763938.01	0	0	5.6×10^{-11}	5.9×10^{-9}	9.7×10^{-13}	1.3×10^{-10}	3.4×10^{-3}	1.8×10^{-6}
228784812.01	4.6×10^{-4}	1.2×10^{-3}	1.2×10^{-4}	1.6×10^{-4}	1.7×10^{-5}	2.0×10^{-5}	8.9×10^{-3}	1.8×10^{-1}
228798746.01	2.9×10^{-4}	4.2×10^{-5}	4.4×10^{-14}	2.8×10^{-8}	1.1×10^{-16}	4.3×10^{-9}	1.4×10^{-1}	2.4×10^{-3}
228801451.01	0	0	2.1×10^{-36}	4.8×10^{-11}	1.6×10^{-16}	7.4×10^{-9}	1.3×10^{-1}	5.6×10^{-8}
228801451.02	0	0	5.5×10^{-11}	2.6×10^{-6}	1.2×10^{-8}	2.1×10^{-8}	1.3×10^{-2}	2.0×10^{-4}
228804845.01	0	0	1.1×10^{-6}	3.5×10^{-8}	8.2×10^{-9}	8.7×10^{-10}	1.5×10^{-2}	7.9×10^{-5}
228809391.01	0	0	3.7×10^{-5}	5.8×10^{-7}	1.7×10^{-7}	3.1×10^{-10}	3.7×10^{-3}	1.0×10^{-2}
228809550.01	3.9×10^{-11}	0	1.0×10^{-7}	9.0×10^{-6}	2.1×10^{-8}	4.4×10^{-7}	1.1×10^{-1}	8.9×10^{-5}
228834632.01	2.3×10^{-5}	3.8×10^{-5}	7.2×10^{-20}	6.6×10^{-10}	2.4×10^{-20}	2.1×10^{-11}	3.5×10^{-3}	1.7×10^{-2}
228836835.01	2.2×10^{-4}	1.7×10^{-3}	3.4×10^{-5}	1.9×10^{-4}	4.2×10^{-6}	2.3×10^{-5}	2.8×10^{-2}	7.4×10^{-2}
228846243.01	0	0	4.7×10^{-5}	4.9×10^{-5}	7.5×10^{-8}	2.3×10^{-7}	7.4×10^{-4}	1.2×10^{-1}
228849382.01	3.7×10^{-8}	0	2.3×10^{-5}	6.8×10^{-5}	2.1×10^{-6}	4.2×10^{-6}	1.3×10^{-2}	7.6×10^{-3}
228849382.02	2.1×10^{-10}	4.4×10^{-10}	7.8×10^{-11}	1.5×10^{-8}	1.6×10^{-11}	7.0×10^{-10}	2.6×10^{-3}	6.2×10^{-6}
228888935.01	0	0	1.1×10^{-8}	9.3×10^{-8}	5.9×10^{-14}	5.7×10^{-14}	3.0×10^{-4}	3.5×10^{-4}
228894622.01	0	0	8.0×10^{-16}	2.1×10^{-12}	2.6×10^{-12}	2.6×10^{-9}	2.1×10^{-1}	1.3×10^{-8}
228934525.01	0	0	4.1×10^{-18}	1.3×10^{-10}	1.6×10^{-19}	3.7×10^{-10}	2.1×10^{-1}	2.3×10^{-9}
228934525.02	0	7.1×10^{-12}	1.3×10^{-34}	1.5×10^{-14}	4.3×10^{-27}	2.5×10^{-13}	5.1×10^{-4}	1.4×10^{-8}
228964773.01	8.3×10^{-11}	0	1.2×10^{-6}	3.4×10^{-6}	1.8×10^{-8}	9.8×10^{-8}	6.0×10^{-4}	7.7×10^{-3}
228968232.01	0	3.1×10^{-11}	5.6×10^{-53}	1.6×10^{-18}	4.0×10^{-68}	1.3×10^{-28}	1.8×10^{-4}	1.7×10^{-7}
228974324.01	0	0	3.7×10^{-186}	7.3×10^{-27}	1.0×10^{-101}	1.1×10^{-29}	1.6×10^{-6}	$< 10^{-13}$
228974907.01	0	0	1.9×10^{-5}	1.1×10^{-5}	7.5×10^{-7}	3.0×10^{-7}	2.6×10^{-3}	1.1×10^{-2}
229004835.01	0	1.6×10^{-11}	7.2×10^{-4}	2.7×10^{-6}	3.8×10^{-6}	9.1×10^{-8}	1.5×10^{-2}	4.5×10^{-2}
229017395.01	0	0	1.9×10^{-9}	4.4×10^{-9}	2.0×10^{-11}	1.8×10^{-9}	1.2×10^{-3}	6.8×10^{-6}
229103251.01	0	0	1.9×10^{-4}	1.3×10^{-4}	4.1×10^{-6}	3.5×10^{-6}	5.1×10^{-3}	6.0×10^{-2}
229131722.01	0	0	6.1×10^{-6}	1.7×10^{-6}	4.0×10^{-7}	8.9×10^{-9}	3.6×10^{-3}	2.3×10^{-3}
229133720.01	0	0	1.2×10^{-25}	8.3×10^{-13}	4.9×10^{-21}	1.3×10^{-12}	4.4×10^{-1}	4.7×10^{-12}

Table 9. WIYN/NESSI datasets used in this work.

EPIC	Filter center [nm]	Filter width [nm]	Obs. Date
201092629	562nm	44nm	2017-05-15
201092629	832nm	40nm	2017-05-15
201092629	562nm	44nm	2017-03-18
201092629	832nm	40nm	2017-03-18
201102594	562nm	44nm	2017-04-05
201102594	832nm	40nm	2017-04-05
201110617	832nm	40nm	2017-03-10
201110617	562nm	44nm	2017-03-10
201111557	562nm	44nm	2017-03-15
201111557	832nm	40nm	2017-03-15
201127519	562nm	44nm	2017-03-11
201127519	832nm	40nm	2017-03-11
201128338	832nm	40nm	2017-03-10
201128338	562nm	44nm	2017-03-10
201132684	832nm	40nm	2017-05-12
201132684	562nm	44nm	2017-05-12
201132684	562nm	44nm	2017-03-15

Table 9 continued

Table 9 *(continued)*

EPIC	Filter center [nm]	Filter width [nm]	Obs. Date
201132684	832nm	40nm	2017-03-15
201164625	562nm	44nm	2017-03-18
201164625	832nm	40nm	2017-03-18
201164625	562nm	44nm	2017-05-12
201164625	832nm	40nm	2017-05-12
201180665	832nm	40nm	2017-03-18
201180665	562nm	44nm	2017-03-18
201211526	832nm	40nm	2017-03-18
201211526	562nm	44nm	2017-03-18
201225286	562nm	44nm	2017-04-03
201225286	832nm	40nm	2017-04-03
201352100	562nm	44nm	2017-03-15
201352100	832nm	40nm	2017-03-15
201357643	562nm	44nm	2017-03-18
201357643	832nm	40nm	2017-03-18
201386739	562nm	44nm	2017-03-17
201386739	832nm	40nm	2017-03-17
201390927	832nm	40nm	2017-03-17
201390927	562nm	44nm	2017-03-17
201392505	832nm	40nm	2017-03-18
201392505	562nm	44nm	2017-03-18
201437844	562nm	44nm	2017-03-11

Table 9 continued

Table 9 *(continued)*

EPIC	Filter center [nm]	Filter width [nm]	Obs. Date
201437844	832nm	40nm	2017-03-11
201595106	832nm	40nm	2017-03-18
201595106	562nm	44nm	2017-03-18
201598502	832nm	40nm	2017-03-18
201598502	562nm	44nm	2017-03-18
228707509	562nm	44nm	2017-04-08
228707509	832nm	40nm	2017-04-08
228720681	832nm	40nm	2017-03-14
228720681	562nm	44nm	2017-03-14
228721452	562nm	44nm	2017-03-11
228721452	832nm	40nm	2017-03-11
228724899	562nm	44nm	2017-03-14
228724899	832nm	40nm	2017-03-14
228725791	562nm	44nm	2017-03-17
228725791	832nm	40nm	2017-03-17
228725972	832nm	40nm	2017-03-17
228725972	562nm	44nm	2017-03-17
228729473	832nm	40nm	2017-04-03
228729473	832nm	40nm	2017-05-19
228729473	562nm	44nm	2017-04-03
228729473	562nm	44nm	2017-05-19
228732031	832nm	40nm	2017-04-05
228732031	562nm	44nm	2017-04-05
228735255	832nm	40nm	2017-03-10
228735255	562nm	44nm	2017-03-10
228736155	562nm	44nm	2017-04-05
228736155	832nm	40nm	2017-04-05
228739306	562nm	44nm	2017-03-09
228739306	832nm	40nm	2017-03-09
228748383	832nm	40nm	2017-03-18
228748383	562nm	44nm	2017-05-19
228748383	832nm	40nm	2017-05-19
228748383	562nm	44nm	2017-03-18
228748826	562nm	44nm	2017-03-09
228748826	832nm	40nm	2017-03-09
228758778	562nm	44nm	2017-04-08
228758778	832nm	40nm	2017-04-08
228758948	832nm	40nm	2017-03-10
228758948	562nm	44nm	2017-03-10
228763938	562nm	44nm	2017-05-19
228763938	832nm	40nm	2017-05-19
228763938	562nm	44nm	2017-03-18
228763938	832nm	40nm	2017-03-18
228801451	832nm	40nm	2017-03-11
228801451	562nm	44nm	2017-03-11
228804845	562nm	44nm	2017-03-10
228804845	832nm	40nm	2017-03-10
228809391	562nm	44nm	2017-03-10
228809391	832nm	40nm	2017-03-10
228809550	832nm	40nm	2017-03-18
228809550	562nm	44nm	2017-03-18
228846243	832nm	40nm	2017-03-17
228846243	562nm	44nm	2017-03-17
228849382	832nm	40nm	2017-05-20
228849382	562nm	44nm	2017-05-20
228888935	832nm	40nm	2017-03-17
228888935	562nm	44nm	2017-03-17
228894622	832nm	40nm	2017-03-09
228894622	562nm	44nm	2017-03-09
228934525	562nm	44nm	2017-03-09
228934525	832nm	40nm	2017-03-09

Table 9 continued

Table 9 *(continued)*

EPIC	Filter center [nm]	Filter width [nm]	Obs. Date
228964773	562nm	44nm	2017-03-18
228964773	832nm	40nm	2017-03-18
228968232	832nm	40nm	2017-03-18
228968232	562nm	44nm	2017-03-18
228974324	832nm	40nm	2017-03-10
228974324	562nm	44nm	2017-03-10
228974907	562nm	44nm	2017-03-18
228974907	832nm	40nm	2017-03-18
229004835	562nm	44nm	2017-03-11
229004835	832nm	40nm	2017-03-11
229017395	832nm	40nm	2017-03-18
229017395	562nm	44nm	2017-03-18
229103251	832nm	40nm	2017-03-09
229103251	562nm	44nm	2017-03-09
229131722	832nm	40nm	2017-05-19
229131722	832nm	40nm	2017-03-10
229131722	562nm	44nm	2017-05-19
229131722	562nm	44nm	2017-03-10
229133720	562nm	44nm	2017-03-11
229133720	832nm	40nm	2017-03-11

Table 11. Predicted atmospheric characteristics, where g is surface gravity, H is atmospheric scale height, and $\delta_{\rm TS}$ is the expected amplitude of atmospheric spectral features.

EPIC	g [$g_\oplus$]	H [km]	$\delta_{\rm TS}$ [ppm]
201092629.01	1.49	133	89
201102594.01	1.53	119	341
201110617.01	1.67	323	127
201111557.01	1.58	255	81
201127519.01	0.57	565	1154
201128338.01	1.63	89	84
201132684.01	1.90	206	42
201132684.02	1.41	233	98
201164625.01	1.51	489	50
201166680.01	1.54	293	43
201166680.02	1.60	218	30
201180665.01	0.30	1077	2765
201211526.01	1.94	134	40
201225286.01	1.56	189	88
201274010.01	1.33	239	94
201352100.01	1.27	212	126
201357643.01	0.80	523	156
201386739.01	1.10	378	197
201390048.01	2.10	123	50
201390927.01	2.04	157	114
201392505.01	1.15	176	141
201437844.01	1.47	301	56
201437844.02	0.95	357	123
201595106.01	1.97	403	70
201598502.01	1.97	96	120
201615463.01	1.38	371	36
228707509.01	0.43	658	1702

Table 11 continued

Table 10. TNG/HARPS-N results.

EPIC	T_{obs} [BJD$_{TDB}$]	RV [km s^{-1}]	BIS [km s^{-1}]	FWHM [km s^{-1}]	log(RHK)	B-V [mag]	T_{exp} [sec]	SNR [5500 nm]
228801451	2457782.629699	22.960809 ± 0.001844	-0.012789	7.175241	-4.5707 ± 0.0098	0.873	1800.0	48.8
201595106	2457782.687224	0.692781 ± 0.002263	-0.022588	6.965865	-4.9714 ± 0.0273	0.703	2400.0	45.0
201437844	2457762.701586	-3.449696 ± 0.005740	0.037015	20.649605	-4.8647 ± 0.0058	0.451	1200.0	101.6
201437844	2457774.738143	-3.441043 ± 0.005931	0.045533	20.699375	-4.8584 ± 0.0060	0.451	1800.0	98.7
201437844	2457774.759707	-3.441611 ± 0.006562	0.073457	20.632207	-4.8629 ± 0.0071	0.451	1800.0	90.0

Table 11 *(continued)*

EPIC	g [$g_\oplus$]	H [km]	δ_{TS} [ppm]
228720681.01	0.51	587	868
228721452.01	1.76	712	54
228721452.02	1.38	431	58
228724899.01	1.14	355	191
228725791.01	1.82	159	168
228725791.02	1.86	109	117
228725972.01	1.43	380	71
228725972.02	1.05	390	116
228729473.01	0.36	1302	248
228732031.01	1.74	515	191
228734900.01	1.00	407	59
228735255.01	0.45	892	1465
228736155.01	1.07	694	68
228739306.01	1.44	250	107
228748383.01	1.56	230	46
228748826.01	1.46	268	141
228753871.01	1.33	194	89
228758778.01	1.83	92	160
228758948.01	0.96	361	185
228763938.01	1.91	135	50
228784812.01	1.84	233	54
228798746.01	2.00	187	74
228801451.01	2.06	379	93
228801451.02	1.58	204	89
228804845.01	1.96	296	50
228809391.01	1.35	197	85
228809550.01	0.55	730	1549
228834632.01	1.99	94	77
228836835.01	1.13	338	406
228846243.01	0.60	555	176
228849382.01	1.96	154	85
228849382.02	1.67	126	92
228888935.01	0.62	612	952
228894622.01	1.29	329	278
228934525.01	1.88	157	125
228934525.02	1.82	126	104
228964773.01	0.83	254	231
228968232.01	1.36	274	157
228974324.01	0.39	688	551
228974907.01	1.18	442	23
229004835.01	1.67	185	50
229017395.01	1.27	273	63
229103251.01	1.23	274	115
229131722.01	1.50	221	55
229133720.01	0.65	1118	185

Table 12. Comparison of parameters between *K2* pipelines.

EPIC	P [days]	ΔP [σ]	R_P [$R_\star$]	ΔR_P [σ]	b	Δb [σ]	a [$R_\star$]	Δa [σ]
201092629.01	$26.809633^{+0.001327}_{-0.001235}$	3.7	$0.0263^{+0.0011}_{-0.0007}$	3.1	$0.25^{+0.28}_{-0.17}$	0.3	$48.0^{+2.0}_{-6.0}$	0.6
201102594.01	$6.513855^{+0.000534}_{-0.000660}$	0.0	$0.0656^{+0.0138}_{-0.0041}$	0.3	$0.54^{+0.37}_{-0.37}$	0.3	$23.0^{+4.3}_{-10.9}$	0.1
201110617.01	$0.813175^{+0.000032}_{-0.000032}$	0.5	$0.0163^{+0.0008}_{-0.0007}$	0.1	$0.39^{+0.33}_{-0.27}$	0.0	$4.6^{+0.5}_{-1.0}$	0.4
201111557.01	$2.302093^{+0.000127}_{-0.000133}$	0.8	$0.0143^{+0.0010}_{-0.0008}$	0.1	$0.40^{+0.34}_{-0.28}$	0.0	$12.0^{+1.5}_{-3.0}$	0.1
201127519.01	$6.178825^{+0.000030}_{-0.000030}$	0.7	$0.1080^{+0.0024}_{-0.0016}$	0.7	$0.24^{+0.15}_{-0.16}$	0.1	$17.7^{+0.4}_{-0.8}$	0.1
201128338.01	$32.652883^{+0.002143}_{-0.002309}$	0.7	$0.0418^{+0.0023}_{-0.0014}$	1.4	$0.40^{+0.32}_{-0.30}$	0.1	$57.0^{+4.8}_{-14.0}$	0.3
201132684.01	$5.898463^{+0.001803}_{-0.001503}$	1.5	$0.0135^{+0.0009}_{-0.0009}$	0.8	$0.30^{+0.23}_{-0.20}$	0.3	$13.3^{+1.3}_{-2.1}$	0.6
201132684.02	$10.062708^{+0.001114}_{-0.001122}$	1.3	$0.0271^{+0.0012}_{-0.0010}$	0.9	$0.43^{+0.22}_{-0.26}$	0.1	$18.9^{+1.9}_{-3.1}$	0.0
201164625.01	$2.713225^{+0.001656}_{-0.001971}$	0.7	$0.0090^{+0.0057}_{-0.0023}$	0.5	$0.47^{+0.37}_{-0.32}$	0.1	$18.8^{+48.6}_{-11.3}$	1.2
201166680.01	$11.540719^{+0.002151}_{-0.002063}$	0.4	$0.0136^{+0.0006}_{-0.0006}$	0.8	$0.43^{+0.16}_{-0.18}$	0.1	$21.0^{+1.0}_{-2.1}$	0.0
201166680.02	$24.942035^{+0.003282}_{-0.003280}$	0.5	$0.0147^{+0.0005}_{-0.0005}$	1.0	$0.22^{+0.26}_{-0.16}$	0.5	$35.0^{+1.7}_{-3.5}$	0.0
201180665.01	$17.773142^{+0.000122}_{-0.000123}$	1.0	$0.1879^{+0.0035}_{-0.0034}$	0.3	$0.67^{+0.02}_{-0.02}$	0.7	$33.6^{+0.5}_{-0.4}$	0.3
201211526.01	$21.073824^{+0.003409}_{-0.002816}$	1.2	$0.0164^{+0.0014}_{-0.0008}$	0.6	$0.40^{+0.35}_{-0.28}$	0.1	$38.0^{+5.9}_{-9.7}$	0.1
201225286.01	$12.420030^{+0.000967}_{-0.000768}$	0.9	$0.0249^{+0.0032}_{-0.0011}$	0.0	$0.40^{+0.37}_{-0.28}$	0.1	$25.8^{+2.2}_{-7.8}$	0.3
201274010.01	$13.008576^{+0.001302}_{-0.001295}$	0.6	$0.0278^{+0.0015}_{-0.0013}$	0.6	$0.42^{+0.34}_{-0.28}$	0.1	$27.7^{+2.9}_{-7.4}$	0.2
201352100.01	$13.383697^{+0.001049}_{-0.001031}$	0.1	$0.0307^{+0.0019}_{-0.0013}$	0.9	$0.41^{+0.33}_{-0.30}$	0.1	$36.4^{+3.6}_{-9.5}$	0.2
201357643.01	$11.893194^{+0.000420}_{-0.000420}$	0.2	$0.0318^{+0.0008}_{-0.0006}$	0.1	$0.36^{+0.32}_{-0.25}$	0.1	$17.7^{+1.1}_{-3.7}$	0.1

Table 12 continued